Tonga Climate Project Final Report

Improved austral winter seasonal forecast and tropical cyclone sub-seasonal to seasonal outlooks in Kingdom of Tonga through APCC MME seasonal prediction

July 2017 • Republic of Korea • Kingdom of Tonga

Tonga Climate Project
Final Report

Contents

APCC
APEC CLIMATE CENTER

METEOROLOGICAL & COAST RADIO SERVICES TONGA

1 Introduction to APCC

— The APEC Climate Center (APCC) is a non-profit organization located in the Republic of Korea that aims to enhance the socio-economic well-being of the Asia Pacific region by utilizing up-to-date scientific knowledge, applying innovative climate prediction techniques, and promoting application of climate information through various programs for capacity building and reducing climate risks in the region. APCC provides assistance to countries in developing and implementing applications of climate information to climate-sensitive sectors like disaster management, agriculture, and water management to improve their performance. In order to enhance the impact of its services, APCC conducts various training programs to assist capacity building in regional developing countries.

APCC was established in 2005 upon its endorsement at the APEC Senior Official Meeting with the mission to enhance the socio-economic well-being of APEC member economies by utilizing up to date scientific knowledge and applying innovative climate prediction techniques. APCC is working towards achieving this mission through our work in climate prediction and climate information services, climate information application and climate change response, and capacity building activities.

Through climate prediction and climate information services, APCC produces and provides value-added, reliable, and timely climate prediction to countries in the APEC region, while serving as a key climate information center to distribute climate data, prediction, and related tools. Through climate information application and climate change response, APCC leads in developing and applying interdisciplinary application techniques, through combining climate and other related sectors to serve social needs and respond to climate change in specific countries and regions. Through capacity building, APCC assists developing economies from the APEC region and beyond in building their capacities to produce reliable climate prediction information and to maintain and utilize APCC products created through the Center's climate information application research.

2 Introduction to the Tonga Climate Project

— The "Improved seasonal forecasts in Tonga during austral winter season through APCC MME seasonal prediction" project (the Tonga Climate Project) was initiated by APCC in partnership with the National Emergency Management Office (NEMO) of the Kingdom of Tonga, or Tonga, and the Tonga Meteorological & Coast Radio Services (TMS, http://www.met.gov.to/). The Tonga Climate Project aims to support more reliable guidance for action plans against possible climate-induced risks in Tonga during the austral winter season.

The tropical Pacific Ocean basin is home to over 20 Pacific Island nations, many of which are sensitive to climate extremes from the El Niño-Southern Oscillation (ENSO) and rainfall variability associated the Inter-Tropical Convergence Zone (ITCZ) and the South Pacific Convergence Zone (SPCZ). These Pacific Island countries are highly dependent on agriculture, fishing, and tourism as a major source of food production and income, which can vary greatly depending on the weather and climate experienced from year to year.

Tropical cyclones also have a significant impact on Pacific Island countries. Historically tropical cyclones have had major impacts on life, agriculture, water supplies, safety, the economy, and in extreme cases, threatened the sustainability of the countries. Better understanding of the year-to-year variability in tropical cyclone frequency and severity is a practical way to decrease current and future vulnerability to tropical cyclones. Although tropical cyclones have significant local impacts in the region, they are known to be predictable on seasonal timescales using dynamical-statistical models, which can make it so that these seasonal forecasts can inform decision-making and planning to improve the resiliency of the Pacific Island countries

Hence, the provision of skillful seasonal forecasts is important to allow these countries to prepare for changes in rainfall and impending droughts associated with the changes in ENSO. APCC has developed a Multi-Model Ensemble (MME) seasonal forecast system, which has been successful at predicting El Niño and La Niña up to several months in advance, and is capable of simulating the spatial and temporal variability of tropical rainfall associated with ENSO. Therefore, APCC MME is expected to improve the seasonal forecasts in Tonga during the dry season. This Tonga Climate Project was proposed to be one of the many collaborative research programs between APCC and TMS. This project aimed to improve the long-range (3 to 6-months as seasonal scales) climate forecasting in Tonga during the dry season, which eventually can support more reliable guidance for action plans against possible climate-induced risks in Tonga during the austral winter season.

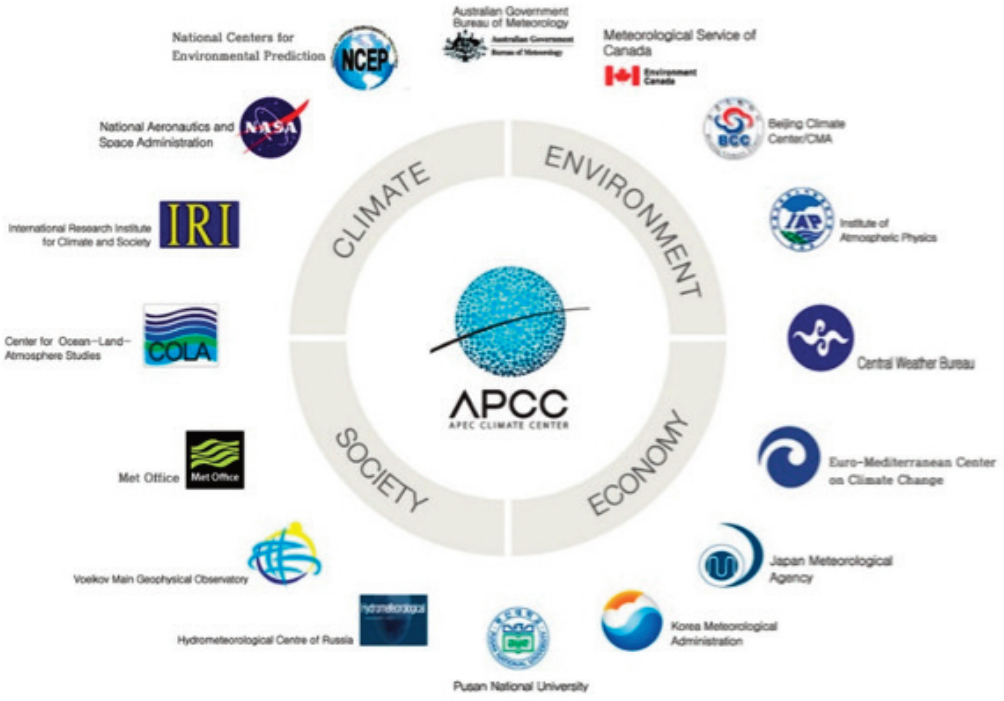

As seasonal climate forecast skill is limited to the performance of the dynamical seasonal prediction, it is significant to be able to identify reliable predictors and incorporate them into the hybrid dynamical-statistical model. This is the key to success in the case of local specific operational seasonal forecast systems. Therefore, this project is attempting to 1) examine the predictability of the APCC MME seasonal forecast system for seasonal climate in Tonga during dry season; 2) understand the predictable source and limitations of dynamical forecast system; and 3) develop a dynamical-statistical downscaling method for seasonal climate in Tonga.

3 Seasonal Forecast during the Austral Winter

3.1 Local and General Features of Tonga's Seasonal Climate

— Tonga consists of several main islands located from low- to mid- latitudes, so the climate in Tonga is influenced by both tropical and extratropical air/sea conditions. Figure 1 shows the location of the six main islands of Tonga, along with the geographical information (latitude, longitude, and elevation) of those islands in Table 1.

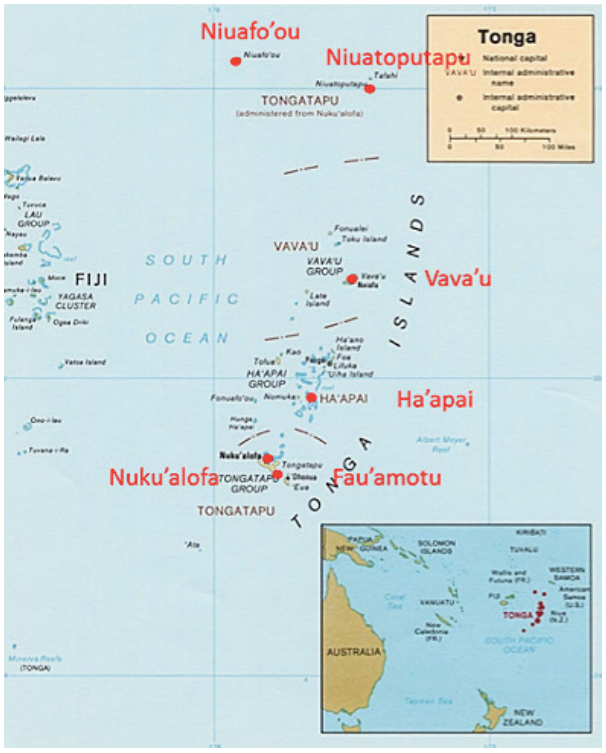

Figure 1.
Location of six main islands of Tonga.

Table 1. Site names and the geographical information of the six islands in the Kingdom of Tonga

	Site Name	Latitude (°)	Longitude (°)	Elevation (m)
1	Niuafo'ou	-15.57	-175.60	60
2	Niuatoputapu	-15.93	-173.77	2
3	Vava'u	-18.58	-173.97	9
4	Ha'apai	-19.80	-174.35	4
5	Nuku'alofa	-21.13	-175.18	2
6	Fu'amotu	-21.25	-175.14	38

Because of the geographical characteristics of the islands in Tonga, each island has its own distinct properties in monthly precipitation. There are two precipitation seasons: wet season (November-April) and dry season (May-October). Figure 2 shows the climatological monthly precipitation in the six islands of Tonga. Monthly variation in climatological precipitation is clear in all six islands. The Northern islands (Niuatoputapu and Niuafo'ou) have larger monthly precipitation variation compared to those of the Central and Southern islands. The Southern islands (Fu'amotu and Nuku'alofa) show relatively evenly distributed monthly precipitation. In particular, the differences in monthly variation of climatological precipitation are small in Ha'apai, Fu'amotu and Nuku'alofa during the dry season.

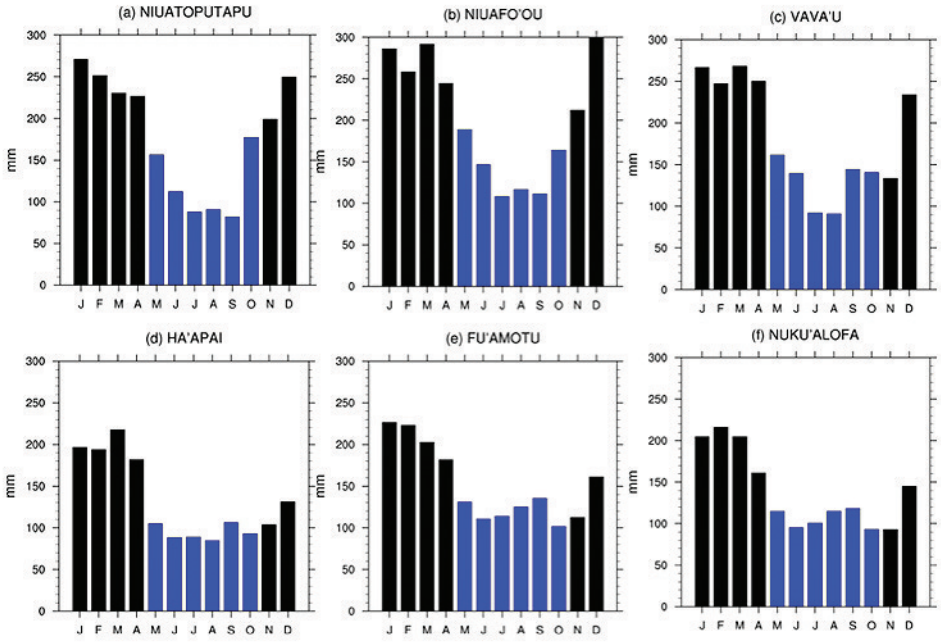

Figure 2. Climatological monthly precipitation in all six islands of Tonga. Black (blue) bars indicate precipitation in the wet (dry) season.

Interannual variability of precipitation is clear in all islands during the dry season (MJJASO, May-October; Figure 3). In the Northern islands, i.e., Niuatoputapu and Niuafo'ou, the ENSO impacts on interannual precipitation variability are more evident compared to those in the other islands. We also found an increasing trend in dry season precipitation, which is more evident in the Southern islands, i.e., Nuku'alofa and Fu'amotu, and the Central island, Vava'u. The increasing trend is not as large as in other islands. Therefore, we have to consider these different characteristics of precipitation variation in each island for the purpose of seasonal precipitation forecasts.

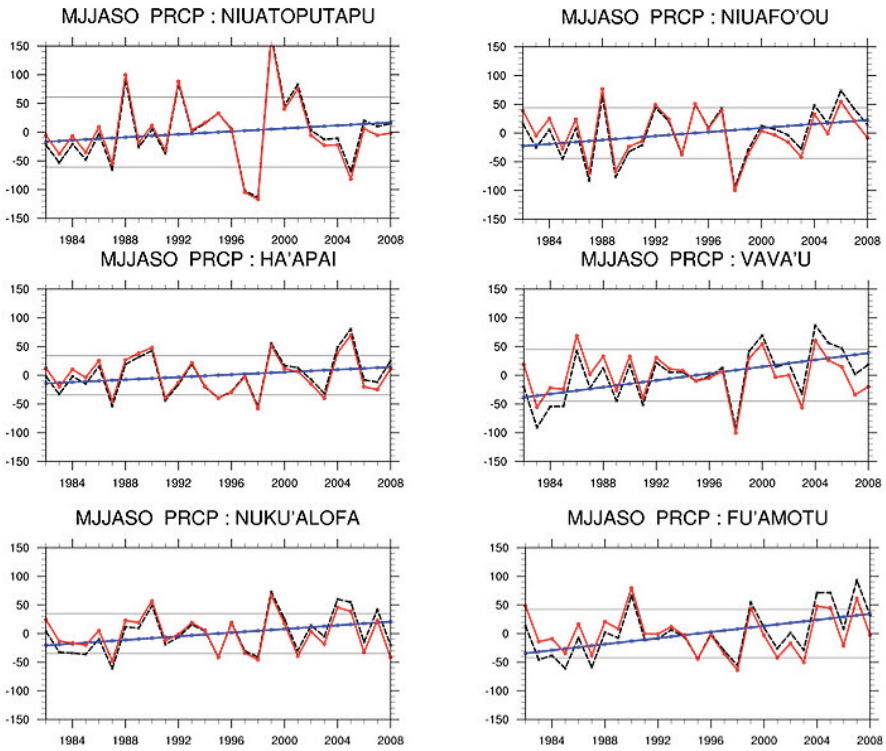

Figure 3. Interannual variability of dry seasonal precipitation in all six islands of Tonga. Black dashed lines indicate precipitation anomalies, blue lines indicate the trends in yearly precipitation, and red lines show de-trended precipitation.

As mentioned earlier, there are various important climate factors that we have to consider for successful pre cipitation prediction in Tonga. Salinger et al. (1995) claimed that five main southwest Pacific precipitation regions show distinctive trends that are connected to the main climatological features. Figure 4 displays the southwest Pacific showing the main climatological features of the area from Salinger et al. (1995). The regional climates are controlled by the oceanic nature and large-scale circulation features, as shown in Figure 4. These include the trade wind regimes, the Hadley and Walker circulations, the seasonally varying, tropical convergence zones, the semi-permanent subtropical high-pressure belt, and the zonal westerlies to the South. The Intertropical Convergence Zone (ITCZ) lies just North of the Equator, and the South Pacific Convergence Zone (SPCZ) lies diagonally from near the Solomon Islands to Samoa, and beyond. These are zones of lower pressure, where converging and rising air produces clouds and rainfall. The variability of the ENSO phenomenon is an important factor of the region's climate at the interannual time scale.

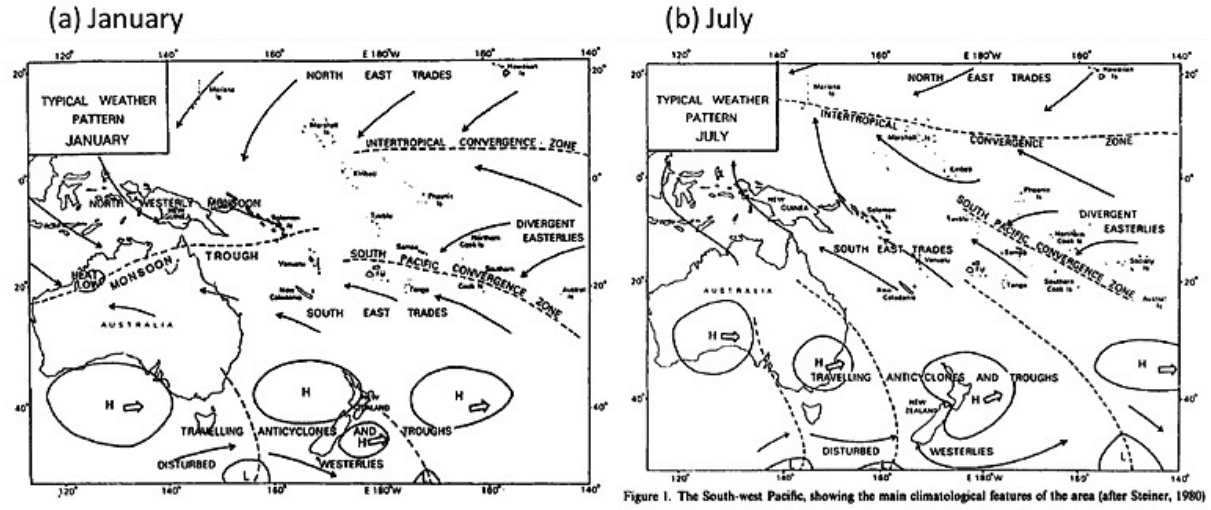

Figure 1. The South-west Pacific, showing the main climatological features of the area (after Steiner, 1980)

Figure 4. The Southwest Pacific, showing the main climatological features of the area (source: Salinger et. al., 1995).

Based on the climatological features of the southwest Pacific, Salinger et al. (1995) classified and defined the regions in the Southwest Pacific that exhibit similar precipitation trends and variability. Figure 5 shows the five regions of the south Pacific that have similar precipitation trends and variability as determined by the cluster analysis. The islands of Tonga are in the P2 (SPCZ) region and P4 (subtropical region). P2 is located in the vicinity of the SPCZ, whose behavior is an important influence on the observed trends. P4 lies to the Southwest of SPCZ and is affected by the migratory anticyclones of the subtropical high-pressure belt. In that region, the annual precipitation anomalies are strongly correlated with the Southern Oscillation Index (SOI). As the result, the position of the convergence zone and the latitude of the subtropical high are considered to be key factors that affect the seasonal climate in Tonga.

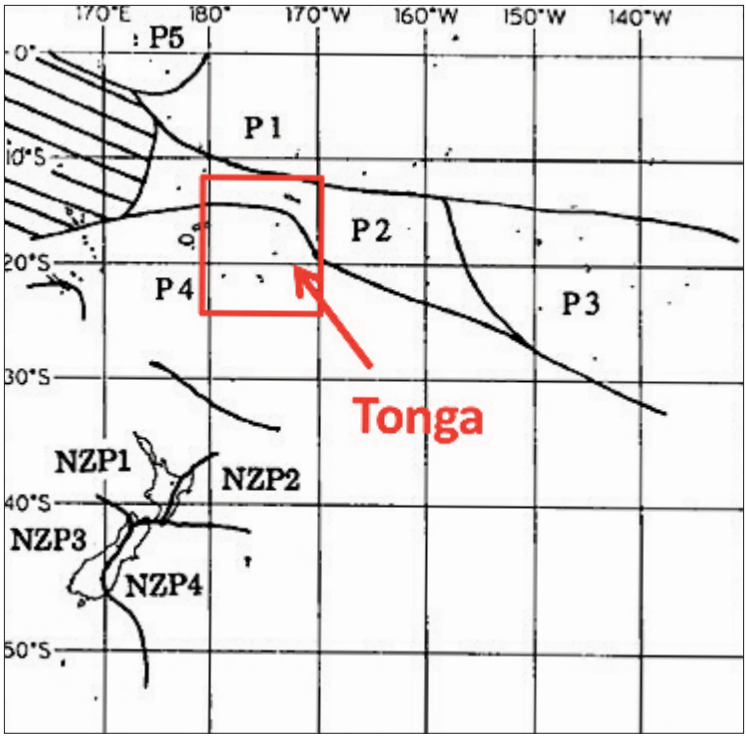

Figure 5. Coherent regions of precipitation trends and variability in the South Pacific (source: Salinger et. al., 1995).

3.2 Current Status of Tonga's Seasonal Climate Forecast

— For operational seasonal forecast in precipitation, TMS has used a statistical model through the Seasonal Climate Outlook for Pacific Island Countries (SCOPIC) system (Abawi et al. 2005). SCOPIC has been used to produce seasonal forecasts in ten Pacific countries since mid-2007 to improve their seasonal forecasting capacity and provide timely warnings to changes in precipitation. Up-to-date monthly precipitation data from each observation point (station) and monthly SOI indices or sea surface temperature anomaly (SSTA) empirical orthogonal functions (EOFs) are used to forecast precipitation. Monthly values of SOI start in January 1876 and start in January 1949 for SSTA EOFs. Some stations have over 100 years of high quality precipitation data available to train the model. However, depending on the selected predictor, not all of the precipitation data is used. The selection of the predictors used by each country and the number of months for the forecast is determined by individual weather services (Cottrill et al. 2013). In SCOPIC, only oceanic variables are considered as potential predictors. Figure 6 shows one snapshot of cross-validation performance of SCOPIC obtained from TMS. It is very clear that the performance of SCOPIC is only as good as climatology, or actually worse than the climatology forecast during the dry season, regardless of which predictor is used for precipitation forecast. Therefore, it is important to develop and improve seasonal forecasting of precipitation in Tonga during the dry season

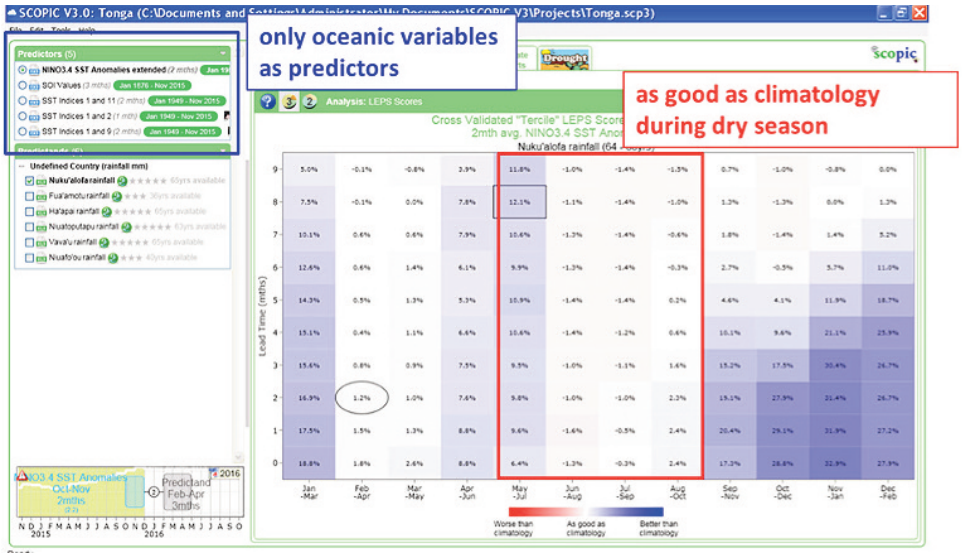

Figure 6. Examples of cross-validated performance of SCOPIC (source: TMS).

3.3 Seasonal Climate Forecast Improvement in Tonga during Austral Winter Season

— APCC has employed the MME seasonal forecast system for several years now. From the viewpoint of seasonal forecasts, the skill of the MME system is higher than that of the single-model component (Palmer et al. 2004). This is the case because MME reduces model errors in individual models by combining ensembles from different agencies, i.e., combining different analyses and forecast models. Therefore, the APCC MME seasonal forecasts are used to develop a seasonal forecast model in this project. Seasonal climate hindcasts and real-time forecasts from seven coupled models, including APCC, Meteorological Service of Canada (MSC), National Aeronautics and Space Administration (NASA) of USA, National Centers for Environmental Prediction (NCEP) of USA, Pusan National University (PNU) of Korea, and Australian Bureau of Meteorology (BOM) from Australia, are used in this study. A brief description of these one-tier prediction models is provided in Table 2.

In this study, we construct the MME using the simple composite method (SCM). In SCM, equal weights are assigned to the ensemble mean prediction of each model under the assumption that each model is relatively independent and has the capability to accurately forecast the climate to some extent. The mean bias from each model is removed by calculating anomalies with respect to each model's own seasonal climatology. We use the hindcasts and real-time forecasts of the seven selected coupled models for the MJJASO season with the initial conditions (ICs) of 1 April (one-month lead seasonal prediction).

Table 2. A brief description of one-tier prediction models used in this project.

Model (Institute)	Resolution	Ensemble member	Hindcast period
CCSM3 (APCC)	T85L26	10	1983-2014
CANCM3 (MSC)	T63L31	10	1981-2010
CANCM4 (MSC)	T63L31	10	1981-2010
GMAO (NASA)	288x181 grid L72	11	1982-2012
CFSv2 (NCEP)	T62L64	20	1982-2010
PNU (PNU)	T42L18	5	1980-2014
POAMA (BOM)	T47L17	33	1983-2011

Seasonal forecasts are made mainly by adopting a dynamical approach or a statistical approach. In the first approach, dynamical information obtained directly from coupled atmospheric-ocean climate models are used for seasonal prediction. In the second approach, empirical predictand-predictor relations based on lagged relationships from previous seasons are employed for seasonal prediction. Here, the predictands (i.e., precipitation) are predicted on the basis of empirically determined relationships by using predictors based on large-scale atmosphere-ocean dynamics (e.g., recent evolution of SSTA). Several publications have focused on the second approach on the basis that model-based predictions of seasonal mean large-scale fields can be used as a set of predictors for the statistical prediction of precipitation. Within the statistical methods, there are two possible approaches. The first statistical calibration method attempts to overcome systematic bias of predicted patterns of climate variability, such as the pattern of precipitation anomaly expected during El Niño. This can be done by adjusting the predicted spatial patterns of variability toward its observed counterpart. The second statistical bridging method is the prediction of a variable, such as precipitation, through its statistical relationships with other model-predicted large-scale climate components, such as temperature or pressure fields. This method attempts to use the model's ability to predict large-scale patterns of variability, such as Southern Oscillation, in order to overcome the model's inability to simulate the associated regional precipitation variability. In this study, we develop a dynamical-statistical model to improve regional precipitation forecast in Tonga through these two distinct methods of statistical post-processing: (1) calibration of direct rainfall prediction patterns from dynamical models (APCC) against observations (CALB), and (2) usage of predicted mean sea level pressure (MSLP) as an atmospheric bridge of the lower boundary forcing to precipitation (BRDG).

We also explore a MME prediction method (ENS) by combining the direct forecasts from APCC and the forecasts from the two statistical-dynamical prediction methods in order to find improved precipitation forecast skill over Tonga. The motivation for exploring ENS is because the overall performance of a multi-model ensemble system is known to be better than the individual component models as a result of offsetting errors and increasing ensemble spread (Lim et al. 2011). As a result, we determined that the ENS is more skillful than the individual component models in regard to forecast reliability, correlation, and error assessments of probabilistic and deterministic forecasts due to the independent information in each of the component models. Figure 7 shows the experimental design and flow chart proposed in this project.

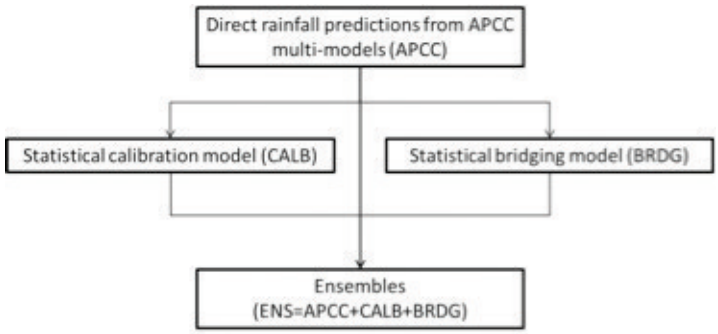

Figure 7. Experimental design proposed for the Tonga Climate Project.

In direct rainfall predictions from APCC multi-models (APCC), monthly climatology rainfall anomalies from both the dynamical forecasts and verification data are seasonally averaged and then normalized by their respective standard deviations at grid points nearest to the observation sites. The dynamical forecast monthly climatology is a function of the forecast start month and lead time. By forming anomalies relative to the model's climatology and standardizing the anomalies relative to the model's variability, some aspects of the mean model bias are removed and the hindcast rainfall is calibrated to have the same standard deviation as observed.

First, the components of the predictors that vary with observed rainfall are identified by using maximum covariance analysis (MCA). This technique expands a predictor field (X) and a predictand field (Y) in terms of their spatial patterns, which maximizes the covariance between the two fields. For the statistical calibration model (CALB), the predictor field is the predicted standardized rainfall anomaly from APCC and the predictand field is the observed standardized rainfall anomaly. By using the relationship between the predictor and predictand, we obtain the predicted standardized rainfall anomaly from CALB. Second, we linearly regress the predictand field (Y) onto the time series of expansion coefficients of a selected number of MCA modes of the predictor, using multiple linear regressions. In this step, we need to set the number of retained MCA modes to include as predictors in this regression model. So we choose three MCA modes in this study. In constructing the statistical-dynamical models, we used all 99 forecast ensemble members by linking them and forming one long time series of predictor field (X) while repeating the predictand time series 99 times to form a compatible long time series of predictand field (Y).

The statistical bridging model (BRDG) is basically based on the same approach as the calibration method (CALB). In the BRDG, however, the predictor field is obtained from the predicted MSLP (0°-75°) anomaly from APCC. The predictand field is the same as the one in BRDG. We use the MSLP as a predictor variable in BRDG because MSLP is directly associated with rainfall. Also, MSLP carries both tropical and extratropical climate mode information such as ENSO, Indian Ocean Dipole (IOD), and Southern Annual Mode (SAM) that are critical drivers of rainfall in the Southern Pacific islands. From this predictor-predictand relationship, we gain the predicted standardized rainfall anomaly from BRDG.

For the ensembles (ENS) in Figure 7, we construct a multi-model ensemble by simply pooling together the rainfall predictions of the two statistical-dynamical models and APCC MME. Although the dynamical-statistical models by themselves do not outperform the direct predictions from APCC MME, they can contribute to skill improvement in the context of MME, provided that there is some independent information in each component models.

Multi-models with a set of ensemble members enable us to perform probabilistic multi-model ensemble (PMME) prediction for the tropical cyclone (TC) numbers. Due to the inconsistency between individual model weights in the hindcast and forecast dataset, forecast probabilities for each tercile category are estimated separately for each model and then are combined into the total probability. We forecast the precipitation in the form of three tercile-based categorical probabilities: above-normal (AN), near-normal (NN), and below-normal (BN), with respect to the climatological rainfall forecasts.

In order to represent the skill of categorical proba bilistic forecasts, WMO recommends the Relative Op erating Characteristics (ROC) score, which is defined as the area under the ROC curve in the plot of hit rates versus false-alarm rates. The area under the ROC curve is frequently used as a score. The ROC curve measures the ability of the forecast to discriminate between two alternative outcomes, thus measuring resolution. It is not sensitive to bias in the forecast,

and therefore does not indicate reliability. A biased forecast can still have good resolution and produce a good ROC curve, which means that it may be possible to improve the forecast through calibration. ROC can thus be considered as a measure of potential usefulness. ROC is conditioned on observations (i.e., given that an event occurred, what was the corresponding forecast?). Therefore, it is a good companion to the reliability diagram, which is conditioned on the fore cast. The ROC curve travels from the bottom left to the top left of the diagram, then across to the top right. A diagonal line indicates no skill. The ROC score ranges from 0 to 1, and a 0.5 score indicates no skill, and a 1 score indicates perfect skill.

The reliability diagram (Wilks 2006), otherwise called the attributes diagram, is widely used as a com pact way of displaying many of the probabilistic fore cast features. The reliability diagram plots the ob served frequency against the forecast probability, where the range of forecast probabilities is divided into K bins (for example, 0-5%, 5-15%, 15-25%, etc.). The sample size in each bin is often included as a his togram or as values beside the data points. Reliability is indicated by the proximity of the plotted curve to the diagonal. The deviation from the diagonal indicates the conditional bias. If the curve lies below the line, this indicates overforecasting (probabilities too high) and points above the line indicate underforecasting (probabilities too low). The flatter the curve in the reliability diagram, the less resolution it has. A forecast of climatology does not discriminate at all between events and non-events, and thus has no resolution. Points between the "no skill" line and the diagonal contribute positively to the Brier skill score. The frequency of forecasts in each probability bin shows the sharpness of the forecast. The reliability is condi tioned on the forecast (i.e., given that an event was predicted, what was the outcome?), and can be expected to give information on the real meaning of the forecast. It is a good partner to ROC, which is con ditioned on observations.

For a probabilistic forecast verification, we also take advantage of the Brier skill score (BSS), which meas ures the improvement of the probabilistic forecast relative to a reference forecast (usually the long-term or sample climatology), thus taking climatological frequency into account. The BSS ranges from -1 to 1, and 0 indicates no skill when compared to the refer ence forecast. The perfect score is 1.

3.3.a) Direct Rainfall Predictions from APCC Multi-Models (APCC)

— As a means of deterministic forecast verification, Figure 8 shows the time-series of the ensemble mean rainfall forecasts from APCC and observed rainfall in Nuku'alofa during JJA from 1983-2009. It is clear that direct precipitation from the APCC model has difficulty in predicting the amount of observed precipitation. During JJA in 1998, as one of the extreme cases, the APCC model can successfully capture the amount of observed precipitation, which is due to the larger influence of the atmosphere/ocean conditions like ENSO. In general, however, the interannual variability in observations is relatively larger, but that in the APCC model is smaller. The temporal correlation coefficient between APCC model predicted precipitation and observation is only 0.10, indicating that there is a room for further improvement for the successful seasonal rainfall forecasts during the dry season.

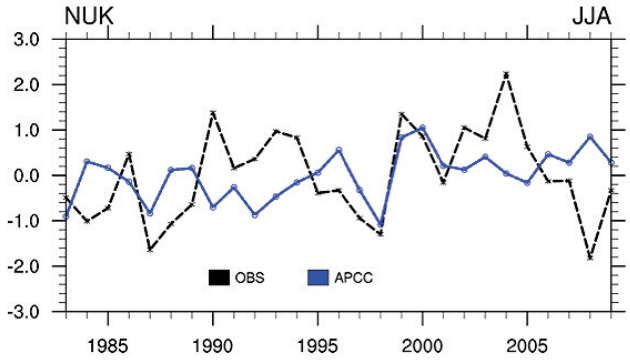

Figure 8. Time-series of the ensemble mean rainfall forecasts from APCC model predicted (blue lines) and observed rainfall (OBS, black lines) in Nuku'alofa during JJA from 1983 to 2009.

We also calculate the temporal correlation coefficient between APCC model predicted and observed rainfall in all six observation sites during the dry season (with three-month running mean from MJJ to ASO). Table 3 summarizes the correlations of the ensemble mean rainfall forecasts from APCC and observed rainfall. The correlation coefficient is very low in general, regardless of the forecast target seasons and observation sites. The correlation coefficients tend to be high in MJJ, but are low in other seasons. In MJJ, there are still moderate signals from the atmosphere/ocean conditions, leading to relatively high correlation coefficients compared to those in other seasons. In JJA, the correlations are very low compared to those in other seasons.

Table 3. Correlations of the ensemble mean rainfall forecasts from APCC and observed rainfall (OBS) in all six observation locations during the dry season with three-month running mean from MJJ to ASO.

	MJJ	JJA	JAS	ASO
Niuafo'ou	0.37	0.08	0.02	0.14
Niuatoputapu	0.38	0.39	0.39	0.40
Vava'u	0.35	0.06	0.32	0.33
Ha'apai	0.40	-0.01	0.26	0.28
Nuku'alofa	0.32	0.10	0.09	0.26
Fu'amotu	0.44	0.21	0.15	0.23

Figure 9a illustrates the ROC curves and reliability diagram calculated from the APCC ensemble mean rainfall forecasts in Nuku'alofa during JJA from 1983-2009. As mentioned earlier, diagonal lines in the ROC curve indicates no skill. The precipitation forecast from APCC models show the lines very close to the diagonal line, which means there is almost no skill in this case. The ROC scores, which defines as the area under the curve, also explain the same result; that is, the ROC scores are 0.49 for above normal (AN), 0.48 for near normal (NN), and 0.60 for below normal (BN). In this case, the performance of APCC MME is far from the perfect forecast. Figure 9b shows the reliability diagram, in which the green areas indicate reliable forecast. However, there are nearly no points for AN and BN, which means the APCC MME precipitation forecast is not reliable in this case. It is found that these same results are repeated regardless of observation sites and forecast seasons.

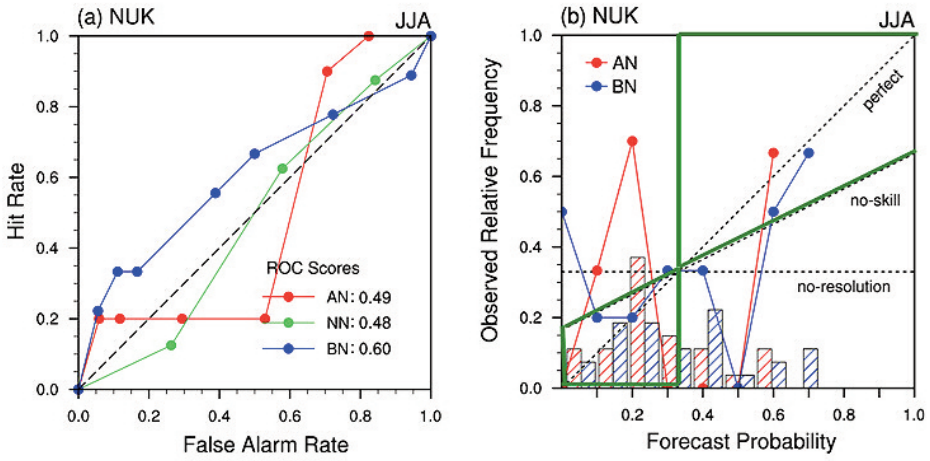

Figure 9. (a) ROC curve and (b) reliability diagram calculated from the APCC ensemble mean rain fall forecasts in Nuku'alofa during JJA from 1983-2009. The red lines are for above nor mal (AN), the green lines are for near normal (NN), and the blue lines are for below normal (BN). The area within the green boundaries in (b) indicates reliable forecast.

We summarized the ROC scores and BSS calculated from the ensemble mean rainfall forecasts from APCC in Nuku'alofa during the dry season with 3-month running means from 1983-2009 (Figure 10). As mentioned earlier, the ROC score of 0.5 indicates no skill and 1 reveals a perfect skill. A BSS of 0 indicates no skill and 1 reveals a perfect skill. As shown in Figure 10, the ROC scores and BSS are far from perfect skill scores, which is independent of forecast category (AN, NN, or BN) and forecast month. There is no big difference among the six observation sites. As shown in the deterministic forecast verification with correlation coefficients, the prob abilistic verification scores are comparatively higher in MJJ compared to those in other seasons. In JJA and JAS, the scores are much close to no skill.

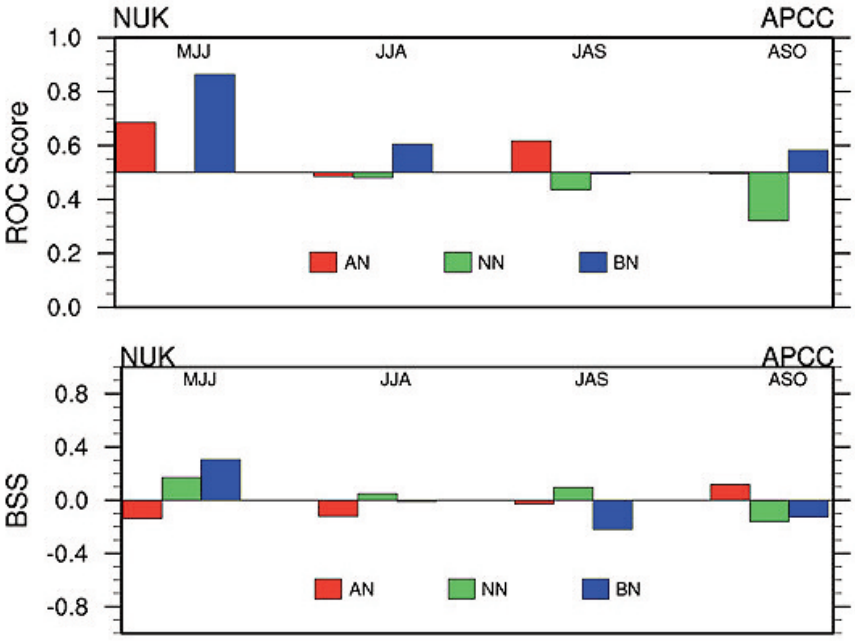

Figure 10. ROC score (upper panel) and BSS (lower panel) calculated from the ensemble mean rain fall forecasts from APCC in Nuku'alofa during the dry seasons with 3-month running means from 1983 to 2009. The red lines are for above normal (AN), green lines are for near normal (NN), and blue lines are for below normal (BN).

3.3.b) Statistical Calibration Model (CALB)

— The rationale for the calibration model is that direct rainfall forecasts from APCC models may suffer from systematic bias as a result of, for instance, a systematic bias in the rainfall teleconnections to Tonga associated with ENSO. In principle, such a bias can be corrected (Lim et al. 2011).

The leading three MCA modes, which explain about 90% of the covariance between dynamically predicted and observed rainfall anomalies in the islands of Tonga, were retained in our statistical calibration model. Table 4 explains how much the leading three MCA modes can explain the total covariance between dynamically pre dicted and observed rainfall during the dry season with 3-month running average. The three modes can explain about 90% of the covariance of dynamically predicted and observed rainfall, regardless of forecast seasons. The first mode can explain the covariability more than 60% during dry seasons. In particular, the first mode can explain 73-75% in MJJ and ASO. The second mode can explain the covariability more than 13% during dry seasons, and it can explain more covariability in JAS. The expansion coefficients of the first three MCA right vectors range from 0.75 to 0.87 in MJJ, from 0.56 to 0.80 in JJA, from 0.66 to 0.84 in JAS, and from 0.64 to 0.84 in ASO, explaining the variance of observed rainfall. The larger amount of explained variance of observed rainfall implies higher predictability by this calibration method, so the predictability is relatively higher in MJJ and lower in JJA compared to other seasons. Overall, the first three MCA time series of dynamically predicted rainfall account for more than 60% and up to 87% of observed rainfall variance in the islands of Tonga.

Table 4. The percentage of how much covariability between dynamically predicted and observed rainfall can be explained by the leading five MCA modes during dry seasons from MJJ to ASO.

%	MJJ	JJA	JAS	ASO
MCA1	73.05	60.18	62.04	75.49
MCA2	13.43	16.69	17.31	14.10
MCA3	5.67	11.78	9.47	4.57
Total	92.15	88.65	88.82	94.16

In constructing the statistical-dynamical schemes, we used all 99 ensemble members (the total number of ensembles of APCC MME) of forecasts by concatenating them and forming one long times series of X while repeating the predictand time series 99 times to form a compatible long time series of Y. A 99-member ensemble hindcast set was produced from each of these models by projecting the 99 members of APCC model rainfall to the calibration model. The statistical-dynamical model was developed with complete cross validation (i.e., the development of the MCA) by leaving out the target in one year, while the models were developed with the data in the remaining years. This process was repeated throughout the entire hindcast period (1983-2009).

As deterministic forecast verification, Figure 11 shows the time-series of the ensemble mean rainfall forecasts from CALB, APCC, and observed rainfall in Nuku'alofa during JJA from 1983-2009. It is clear that the APCC direct precipitation prediction model has difficulty in predicting the amount of observed precipitation, and forecast skill of CALB is overall not as good as that of the APCC direct rainfall prediction over most areas. The reason for the overall poorer performance of the statistical-dynamical models is likely to be related to the strict cross-validation process: we are attempting to correct a relatively modest signal using a short record of hindcasts. The performance of rainfall forecast from CALB statistical model is different from region to region, and from season to season (Figure 11 and Figure 12).

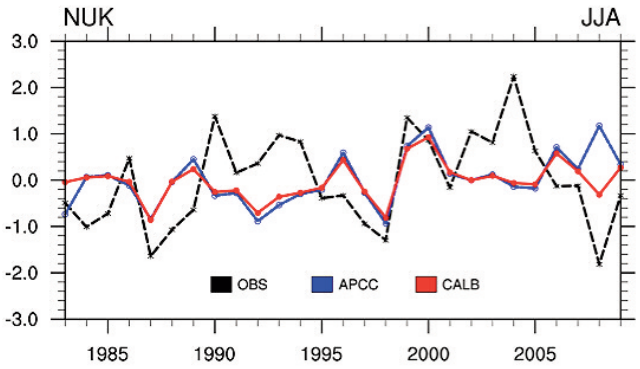

Figure 11. Time-series of the ensemble mean rainfall forecasts from APCC (blue lines), CALB model predictions (red lines), and observed rainfall (OBS, black lines) in Nuku'alofa during JJA from 1983 to 2009.

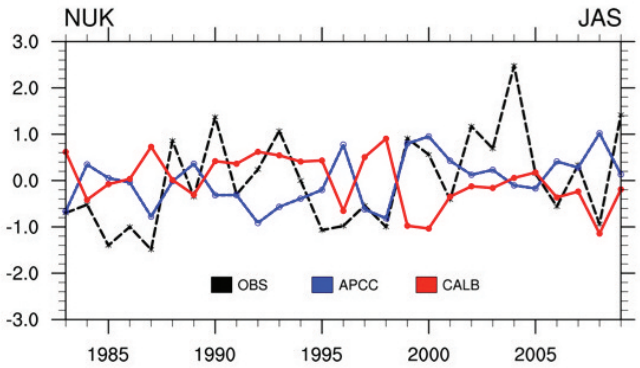

Figure 12. Time-series of the ensemble mean rainfall forecasts from APCC (blue lines), CALB model predictions (red lines), and observed rainfall (OBS, black lines) in Nuku'alofa during JAS from 1983 to 2009.

Forecast skill, as measured by ROC and BSS, from the CALB model is lower than or similar to that from the APCC direct rainfall prediction in most regions (Figure 13). The poorer performance of the statistical calibration model suggests that the major source of errors in APCC rainfall forecasts is unlikely to be the model's systematic linear bias, which should be corrected statistically, in principle. This result suggests that our hindcast record is probably too short in order to develop stable statistical corrections. For instance, during the period 1983-2009 we sample only a handful of El Nino and La Nina events, which are the primary drivers of climate variability in the islands of the Pacific Ocean.

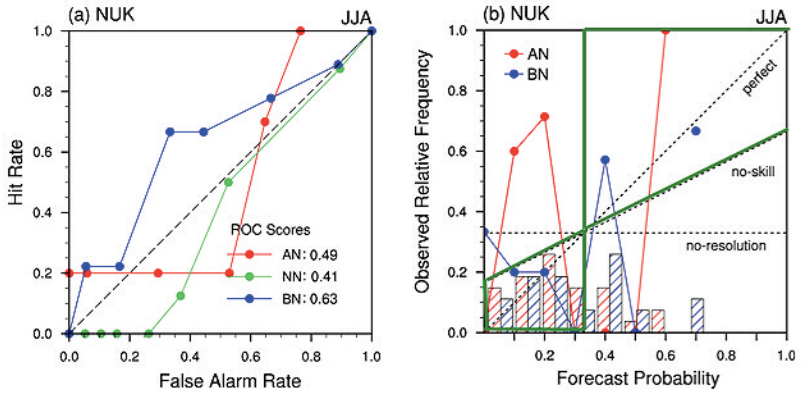

Figure 13. (a) ROC curve and (b) reliability diagram calculated from the ensemble mean rainfall forecasts from CALB in Nuku'alofa during JJA from 1983-2009. The red lines are for above normal (AN), green lines are for near normal (NN), and blue lines are for below normal (BN). The area with green boundaries in (b) indicates reliable forecast.

3.3.c) Statistical Bridging Model (BRDG)

— The rationale for the bridging scheme is that APCC models may have some skill in predicting the large-scale variations of circulation that exert a strong control over local rainfall (Lim et al. 2011). As mentioned earlier, we have chosen MSLP as a predictor variable because MSLP is directly associated with rainfall. Also, MSLP carries information of both tropical and extratropical climate modes such as ENSO and IOD that are important drivers of rainfall of the islands in Tonga. Predictor field (X) in the statistical bridging model is a dynamically predicted MSLP anomaly pre-filtered by projecting the APCC forecasts onto the leading 10 empirical orthogonal function modes of the observed MSLP. Pre-filtering of MSLP data with EOF analysis reduces the number of degrees of freedom in the MSLP field, and therefore, can result in more stable SVD modes.

The 10 leading EOFs of observed MSLP (weighted by square root of cosine latitude) explain about 90% of the total MSLP variability in dry season in the SH tropics-extratropics (0°-75°), according to our analyses on the NCEP-DOE reanalysis (Kanamitsu et al. 2002). The first four observed EOF modes of MSLP explain about 60% of the total variance and are shown in Figure 14. The first observed EOF mode (EOF1) represents SAM (Thomp son and Wallace 2000). The second observed EOF mode of MSLP shows the wave train pattern that is commonly referred to as the Pacific-South American Pattern (PSA; Mo and Paegle 2001; Mo and Higgins 1998). The PSA modes refer to two leading modes of variability in the extratropics, linking tropical and extratropical climates. The mode exhibits well-defined wave trains extending from the tropical Pacific Ocean to South America (Mo and Paegle 2001). The dynamics and mechanisms of decadal variability of the PSA modes over the 20th century are revealed in recent study (Zhang et al. 2016).

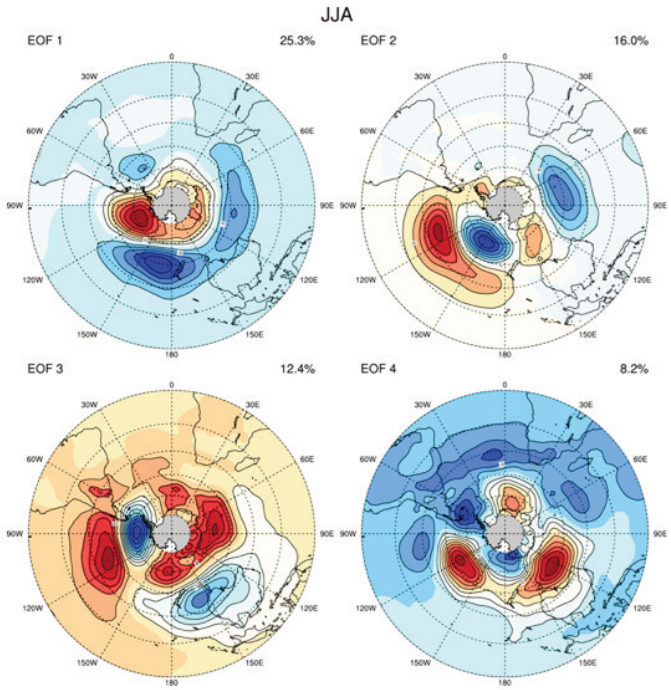

Figure 14. First four EOF patterns obtained by regression of observed MSLP field onto the standardized PCs in the period of 1983-2009 from the NCEP-DOE reanalysis II dataset. The domain is 0°-75°S. The red (blue) contour indicates positive (negative) loadings. The percentage at the top right of each map is MSLP variance accounted for by each mode.

In constructing the statistical bridging-dynamical schemes, we used all 99 ensemble members (as in the calibration statistical model) of forecasts by linking them and forming one long times series of X, while repeating the predictand time series 99 times to form a compatible long time series of Y. A 99-member ensemble hindcast set was produced from each of these models by projecting 99 members of the APCC model rainfall to the bridging model. The statistical bridging-dynamical model was developed with complete cross validation (i.e., including the development of the EOFs and MCA) by leaving out the target one year while the models were developed with the data in the remaining years. This process was repeated throughout the entire hindcast period (1983-2009).

As deterministic forecast verification, Figure 15 shows the time-series of the ensemble mean rainfall forecasts from BRDG, APCC, and observed rainfall in Nuku'alofa during JJA from 1983-2009. It is clear that direct precipitation from the APCC model has difficulty in predicting the amount of observed precipitation, and the forecast skill of BRDG is generally not as good as that of the APCC direct rainfall prediction over most areas. As indicated in the CALB results, the reason for the overall poorer performance of the statistical-dynamical models is likely related to the strict cross-validation process: we are attempting to correct a relatively modest signal using a short record of hindcasts. The performance of rainfall forecast from BRDG statistical model is different from region to region, and from season to season (Figure 15 and Figure 16).

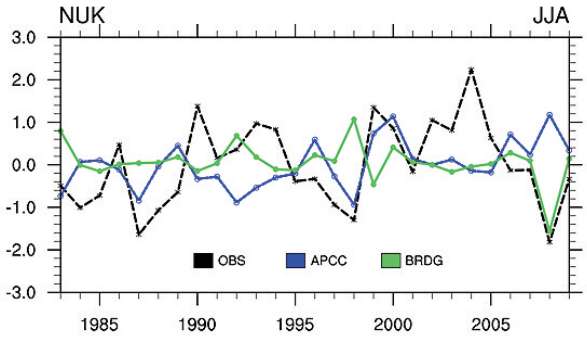

Figure 15. Time-series of the ensemble mean rainfall forecasts from APCC (blue lines), BRDG model predicted (red lines), and observed rainfall (OBS, black lines) in Nuku'alofa during JJA from 1983 to 2009.

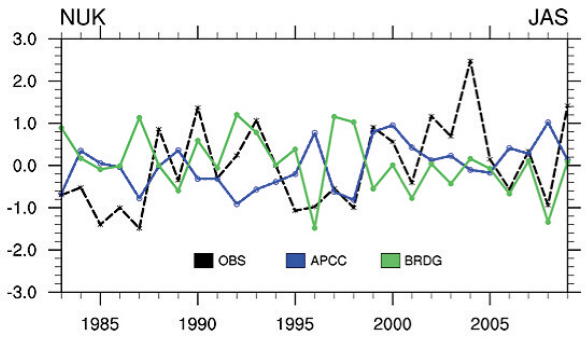

Figure 16. Time-series of the ensemble mean rainfall forecasts from APCC (blue lines), BRDG model predicted (red lines), and observed rainfall (OBS, black lines) in Nuku'alofa during JAS from 1983 to 2009.

Forecast skill, as measured by ROC and BSS, from the BRDG model is lower than or similar to that from the APCC direct rainfall prediction in most regions (Figure 17). As mentioned in the CALB result, the poorer performance of the statistical bridging model suggests that the major source of errors in APCC rainfall forecasts is unlikely to be the model's systematic linear bias, which should be corrected statistically, in principle. This result suggests that our hindcast record, again, is probably too short in order to develop stable statistical

corrections. Also, in the case of constructing a statistical bridging model, it is difficult to find a dominant predictor variable to explain the variability of rainfall over the islands of Tonga and in all seasons. Tropical SST might be a reasonable strong empirical relationship between Tonga rainfall and ENSO, which should be considered in a future study.

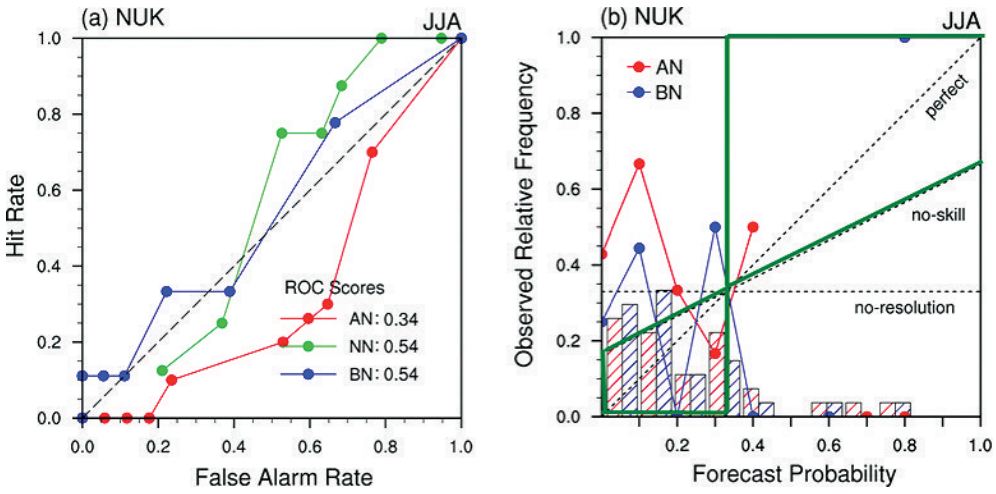

Figure 17. (1) ROC curve and (b) reliability diagram calculated from the ensemble mean rainfall forecasts from BRDG in Nuku'alofa during JJA from 1983-2009. The red lines are for above normal (AN), green lines are for near normal (NN), and blue lines are for below normal (BN). The area with green boundaries in (b) indicates reliable forecast.

3.3.d) Ensembles (ENS)

— Although the statistical-dynamical models by themselves do not outperform the APCC direct predictions, they can contribute to skill improvement in the context of a multimodel ensemble (ENS), provided that there is some independent information in each component model (Doblas-Reyes et al. 2000; Zebiak 2003; Hagedorn et al. 2005). Some indication of the independence of the three forecast sets is shown in Figure 8, Figure 11, and Figure 15, which display the time-series of the rainfall forecasts from APCC, CALB, and BRDG. The correlation of the ensemble mean rainfall anomaly from CALB (BRDG) with the APCC direct prediction is 0.8 (-0.5). While the BRDG forecasts are clearly largely independent (low correlation) from the direct predictions, the CALB forecasts are strongly related with the direct predictions in Nuku'alofa in JJA. About 20% of the variance of the calibrated forecasts is unexplained by the direct predictions in the region and the unexplained variance is different from region to region and from season to season. We therefore constructed a 30-member homoge neous multi-model ensemble (ENS) by simply pooling together the rainfall predictions of these two statistical -dynamical models (CALB and BRDG) and APCC (99 ensemble members from each single model).

Figure 18 shows the reliability diagram of ENS predictions at Fu'amotu during JJA. ENS forecast reliability is marginally better or similar compared to the APCC direct rainfall prediction reliability. The improvement of forecast reliability is clearer in the BN than in AN and NN. The improvement revealed in the reliability diagram is different from region to region and from season to season. Figure 19 shows the ROC curve of the ENS predictions at Fu'amotu during JJA. The larger value of the ROC score is clear in BN, but has a smaller value in AN and NN. Our study suggests that even if statistical or statistical-dynamical forecasts are not very skillful, they can still contribute to improving seasonal forecast skill as components of a multi-model ensemble system. More complex methods of combining models (e.g., Bayesian approach) might be able to stretch the skill of the ENS further, which is worth investigating in a future study.

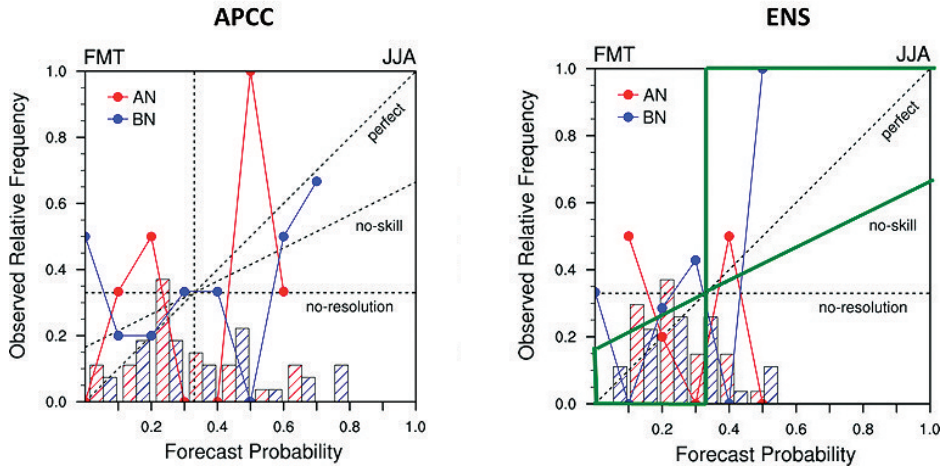

Figure 18. Reliability diagram calculated from the ensemble mean rainfall forecasts from (left) APCC and (right) ENS in Fu'amotu during JJA from 1983-2009. The red lines are for above normal (AN), and blue lines are for below normal (BN). The area with green boundaries in (b) indicates reliable forecast.

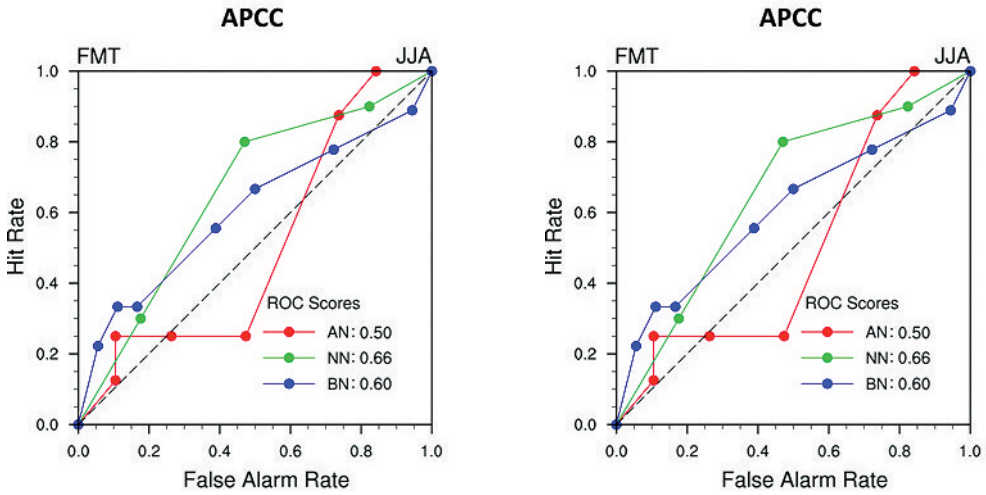

Figure 19. ROC curve calculated from the ensemble mean rainfall forecasts from (left) APCC and (right) ENS in Fu'amotu during JJA from 1983-2009. The red lines are for above normal (AN), green lines are for near normal (NN), and blue lines are for below normal (BN). The numbers in the bottom right in each panel indicate ROC scores for each category.

4 Tropical Cyclone Subseasonal and Seasonal Prediction

4.1 Seasonal Tropical Cyclone Forecast

— Skillful prediction of tropical cyclone (TC) activity can be of great benefit for emergency preparedness and disaster mitigation in many coastal regions. Because of the short lead time for generating forecasts of a few days, high-resolution numerical weather forecast models are used to provide skillful forecasts for the genesis and tracking of individual TCs. Beyond this time scale, however, the nature of the atmosphere makes it impossible for forecasters to focus on individual TCs, but rather on the statistics of TC activity, such as their genesis or frequency. With the improvement in seasonal climate prediction and seasonal TC forecasts, many studies have been devoted to successful TC activity forecasts on seasonal time scales in various basins.

Various forecast centers have issued and shared information on seasonal TC activity in the South Pacific with lead times of several months. The Bureau of Meteorology (BoM, Australia) has issued statistical seasonal TC forecasts for the South Pacific (http://www.bom.gov.au/cyclone/). Once a year, in early October, BoM provides seasonal TC frequency information for the broad western and eastern region of the entire South Pacific. Their model has a good level of accuracy in predicting TC numbers in the western region, but a very low level of accuracy for the eastern region, and a low level of accuracy for the South Pacific region (Kuleshov et al. 2009). The European Centre for Medium-Range Weather Forecasts (ECMWF, UK) also provides dynamical seasonal forecasts of TC frequency for the entire South Pacific. Their information includes a single value for forecast mean and standard deviation of TC frequency for the entire South Pacific. Unfortunately, the seasonal forecast of TCs is only available to ECMWF member states and WMO users. The Fiji Meteorological Service (FMS/RSMC-Nadi, Fiji) also announces the TC seasonal outlook every October, once a year. The outlook is prepared by New Zealand's National Institute of Water & Atmospheric Research (NIWA) and Meteoro logical Service of New Zealand (MetService), along with meteorological forecasting organizations from the Southwest Pacific, including the Australian BoM, and the Pacific Island National Meteorological Services (http://www.met.gov.fj/). These aforementioned centers regularly provide seasonal TC outlooks for the South Pacific, but it is still necessary to produce and deliver more value-added and reliable seasonal TC activity information. As the APCC multi-model ensemble (MME) seasonal forecast system has improved over the last several years, the development of a seasonal TC activity prediction system based on the APCC MME forecast will be a way to produce value-added and reliable seasonal TC information for the South Pacific.

Seasonal TC forecasts are made by adopting a dynamical approach or a statistical approach. In the first approach, dynamical information obtained directly from coupled atmospheric-ocean climate models are used for seasonal TC predictions. TCs are identified and tracked on the basis of the definition of the criteria, i.e., the thresholds and domain over which they are computed. Fully coupled high-resolution global circulation models (GCMs) are essential to this approach. In the second approach, empirical predictand-predictor relationships based on lagged relationships from previous seasons are employed for TC prediction. Here, the predictands (i.e., TC activity) are predicted on the basis of the empirically determined relationships by using predictors based on large-scale atmospheric-ocean dynamics (e.g., recent evolution of El Niño Southern Oscillation, ENSO). Werner and Holbrook (2011) developed a seasonal forecast model of TC for mation in the Australian region based on Poisson regression using the Bayesian approach.

Based on the consideration that model-based predictions of seasonal mean contemporaneous large-scale fields can be used as a set of predictors for the statistical prediction of TC activity, several works have recently focused on the hybrid statistical -dynamical technique. Wang et al. (2009) made the first attempt to build an empirical relationship between the observed interannual variability of hurricanes in the Atlantic and the variability of sea surface temperature (SST) and vertical wind shear (VWS) in 26 years (1981-2006) of hindcasts from the National Centers for Environmental Prediction (NCEP) Climate Forecast System (CFS). Kim and Webster (2010) furthered this study and developed a hybrid forecast model of the seasonal hurricane activity in the North Atlantic. Their model combined ECMWF hindcasts (29 years, 1981-2009) and an empirical model to forecast extended-range seasonal hurricane numbers for the North Atlantic. Kim et al. (2012) also employed the hybrid statistical-dynamical technique to develop a track-pattern-based model for the prediction of seasonal TC activity in the western North Pacific (WNP). They used seasonal large-scale information from the NCEP CFS retro spective forecasts to develop the hybrid statistical -dynamical model. These studies showed that the forecasting skill of the hybrid forecast model was better than or at least comparable to that of other publicly available models. In this study, therefore, we focus on the development of such an approach for predicting the seasonal TC activity in the South Pacific.

The observational TC location data used in this study are archived at the International Best Track Archive for Climate Stewardship (IBTrACS) (Knapp et al. 2010) maintained by the National Climate Data Center (NCDC). IBTrACS is a global data archive that combines best track data from WMO-sanctioned forecast agencies, including various Regional Specialized Meteorological Centers (RSMCs) and Tropical Cyclone Warning Centers (TCWCs) from around the world. The best track data at IBTrACS for the South Pacific are maintained by RSMC-Nadi and TCWC of Wellington. Using the best track data from IBTrACS, we calculate TC genesis frequency in the South Pacific covering 140°E–130°W longitude and 5°S–40°S latitude. In this study, TCs over tropical depressions (TD) (see WMO 2014, see Figure 20) during NDJFMA (November to April) from 1982/1983 to 2008/2009 are considered.

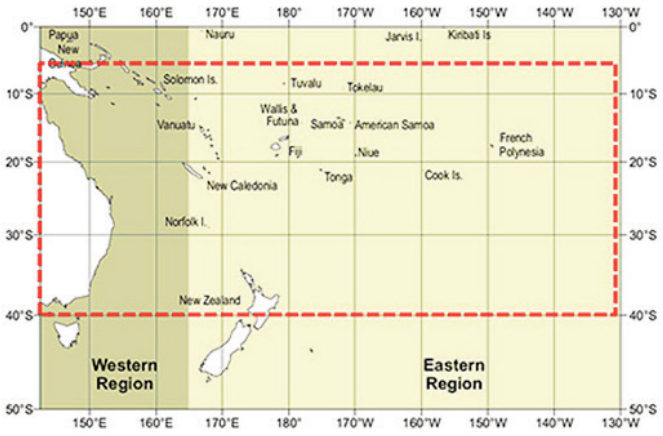

Figure 20. TC genesis region in the South Pacific between 140°E–130°W and 5°S–40°S, (right) operational terminology for TCs used in the South Pacific (WMO 2014).

Figure 21 exhibits annual and monthly variations of TC occurrences from 1982/1983 to 2008/2009, which are calculated using TCs defined as above. The interannual variability is clear in that more TCs tend to occur in El Niño years (Figure 21a). This indicates that ENSO phases have a strong influence on TC activity in the South Pacific; in other words, the ENSO phase can be considered as a significant indicator or predictor for seasonal TC activity in the South Pacific. The number of TCs each month indicates that most TCs have occurred in November through April each year. In particular, January-March is the main period for TC occurrence in the South Pacific (Figure 21b).

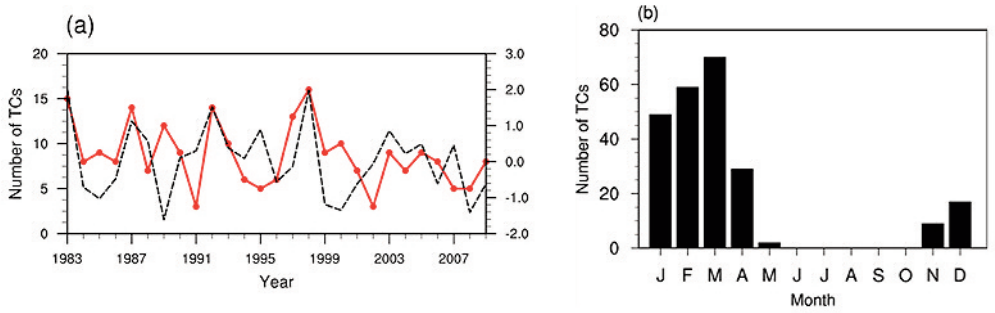

Figure 21. (a) Annual and (b) monthly variation of TC occurrence from 1982/1983 to 2008/2009 (27 years). In (a) a red solid line indicates TC occurrence, and a black dashed line represents ENSO index (Niño-3.4 index).

The observed SST and wind data covering the 27-yr period (1982/1983-2008/2009) are from the Extended Reconstructed SST version 3 (Smith et al. 2008) and NCEP-NCAR Reanalysis II (Kanamitsu et al. 2002) on a 1° (longitude) by 1° (latitude) grid, and a 2.5° (longitude) by 2.5° (latitude) grid, respectively. The other parameters used are sea level pressure (SLP), zonal wind at 850 (U850) and 200 hPa (U200), relative vorticity at 850 hPa (VOR), and vertical wind shear (VWS), which is defined as the difference in zonal wind between 200 hPa and 850 hPa (U200-U850).

Seasonal climate hindcasts and real-time forecasts from five independent coupled models from the Meteor ological Service of Canada (MSC), National Aeronautics and Space Administration (NASA) of USA, the National Centers for Environmental Prediction (NCEP) of USA, and Pusan National University (PSA) of Korea are used in this study. A brief description of these one-tier prediction models is provided in Table 5. In this study, we con struct the MME using the simple composite method (SCM). In SCM, equal weights are assigned to the ensemble mean prediction of each model under the assumption that each model is relatively independent and that each has the capability to accurately forecast the climate to some extent. The mean bias from each model is removed by calculating anomalies with respect to each model's own seasonal climatology. We use the hindcasts for 27 yrs (1982/1983-2008/2009) from the five selected coupled models for the austral summer season with the initial conditions in October each year.

Table 5. Description of APCC one-tier prediction models; note that the common hindcast period among models is 1982/1983-2008/2009 (27 yrs) and the number of ensembles is also given.

Model (Institute)	AGCM (resolution)	OGCM (resolution)	Ensemble Member	Hindcast period
CCCma CGCM3 (MSC)	AGCM3 (T63L31)	OGCM4 (1.41°lon x 0.94°lat L40)	10	1981–2010
CCma CGCM4 (MSC)	AGCM4 (T63L31)		10	1981–2010
CFSv2 (NCEP)	GFS (T126L64)	MOM4/OM (lat 1° x lon L40)	20	1982–2008
PNU (PNU)	CCM3 (T42L18)	MOM3 (0.7~2.8 lat L29)	5	1980–2012
GMAO (NASA)	GEOS-5 (288x181L72)	MOM4 (720 x 410 L40)	11	1982–2012

Figure 22 is a diagram showing the flow of seasonal TC prediction in the South Pacific using the APCC MME. The procedure for forecasting seasonal TCs consists of pre-processing, running the main model, and post-processing. During pre-processing, we per form a cluster analysis to obtain a reasonable number of clusters of TC best tracks in the South Pacific. In this step, we acquire the seasonal TC numbers for each cluster (i.e., predictand). In the next step of run ning the main model, we select a best set of predic tors for each cluster and establish the empirical model between the predictors and predictand. Since the simultaneous large-scale atmospheric and oceanic fields explain the seasonal TC activity in the South Pacific, it is important to examine how the interannual variability of observed seasonal TCs is related to the observational environmental fields as potential predictors. We then analyze the prediction skill of the APCC MME hindcasts for the large-scale variables. The APCC MME hindcast prediction skill for the variables during the austral summer season is cross validated by correlating APCC MME hindcasts anomalies with both the observation fields and observed TC numbers. We then establish the empirical model between the predictors and predictand.

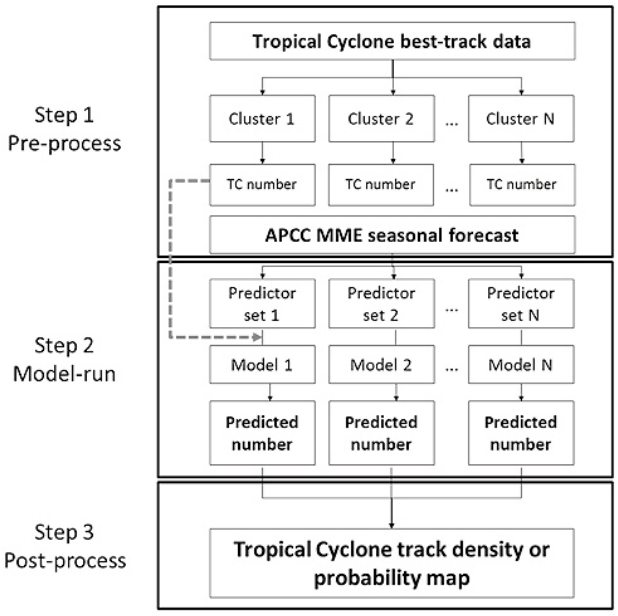

Figure 22. Flowchart of cyclone-track-based seasonal tropical cyclone prediction using APCC MME prediction.

In the final step, we construct the forecasting map of seasonal tropical cyclone track density, which will be included in the seasonal tropical cyclone outlook. From the empirical model using the APCC MME forecasts, we can obtain as many results as the number of clusters. Therefore, we need to employ a combining technique to construct the forecasting map of seasonal TC tracks in the South Pacific. In this study, we employ a construction method to obtain the forecasting map of seasonal TC track density developed by Kim et al. (2012). This method has been adopted for operational work at the National Typhoon Centre in Jeju, Korea. Based on this method, we can finally obtain (1) a map of seasonal TC track density for a target year, and (2) a map of seasonal TC track deviation for a target year compared to that of a normal year. Considering the active TC season in the South Pacific from November to April and the availability of the APCC MME forecasts, the seasonal TC track density map will be produced on a year, in October.

In the pre-processing, we employ a cyclone track clustering technique proposed by Gaffney (2004) to separate the whole TC tracks into several groups. The mode is a regression mixture model, and accommodates cyclone tracks of variable lengths. It can thus handle TC tracks of different trajectory shapes and locations in the modeling process, which is one of the main advantages of the cluster technique over others. A detailed description of the clustering method is provided in Gaffney et al. (2007). The clustering technique has been applied to TC tracks in various basins, for example, the western North Pacific (Camargo et al. 2007a, b), eastern North Pacific (Camargo et al. 2008), North Atlantic (Kossin et al. 2010), and Fiji-Samoa-Tonga (FST) region (Chand and Walsh 2009).

We examine general characteristics of TCs in each cluster for three clusters. Figure 23 shows the TC genesis position and cumulative track density (number of TCs per 5° × 5° grid) in each cluster. The genesis locations of cluster C are very close to the northeastern part of Australia, and those of cluster B are concentrated on the Coral Sea. Cluster A show the maximum genesis locations around the dateline and farther east. In general, the major climatological features of TC activity are clear, such as the lack of systems toward the cold tongue in the eastern Pacific and high activity in the Coral Sea (e.g., Dowdy et al. 2012).

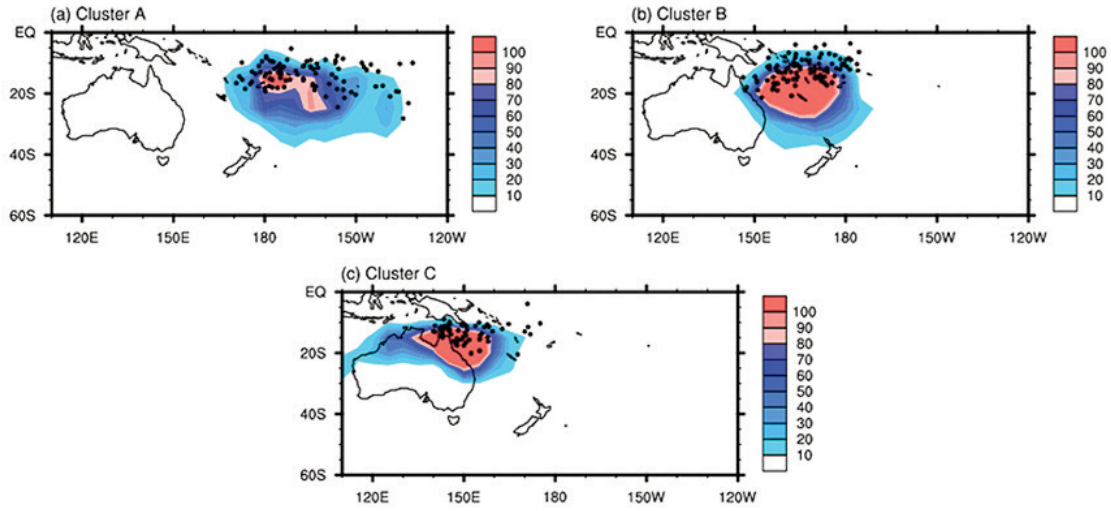

Figure 23. TC genesis position (black dots) and track density (color shaded) in each cluster for 234 TCs in the South Pacific in the period 1983/1984 to 2008/2009; TC genesis position is defined as the first geographical point (latitude and longitude) recorded in IB TrACS, and the track density is defined as the number of TCs during their whole lifetime per 5° × 5° grid, with 9-point smoothing.

It is well known that the key driver of TC interannual variability in the South Pacific is ENSO. ENSO modulates the lower tropospheric source of vorticity and changes the vertical wind shear profile, consequently affecting TC activity. For instance, Ramsay et al. (2008) suggested that vertical zonal wind shear (850–200 hPa) and low -level vorticity are the major ENSO-related factors affecting TC occurrence in the Australian region. Chand and Walsh (2009) also found variations in TC genesis positions for different phases of ENSO, and indicated that favorable TC genesis positions in the FST region are observed when large-scale environments have seasonal average thresholds of 850 hPa cyclonic relative vorticity and 200 hPa divergence, and environmental vertical wind shear. As such, we find that reasonable ENSO predictability in models will assist in improving seasonal outlooks and TC impact information for the people of the South Pacific region.

We examine how the interannual variability of TCs in the South Pacific is related to the observed SST. Figure 24 exhibits the contemporaneous correlation patterns of the TC number in the whole basin with the observed SST in November-April. The pattern is an indicator of ENSO, in which positive (negative) correlations are obvious over the eastern equatorial Pacific (western and southern Pacific). In particular, the TC's relationship with the warm phase of ENSO is clear in the eastern Pacific. Many previous studies have demonstrated that cyclogenesis in the South Pacific is related to the warm phase of ENSO.

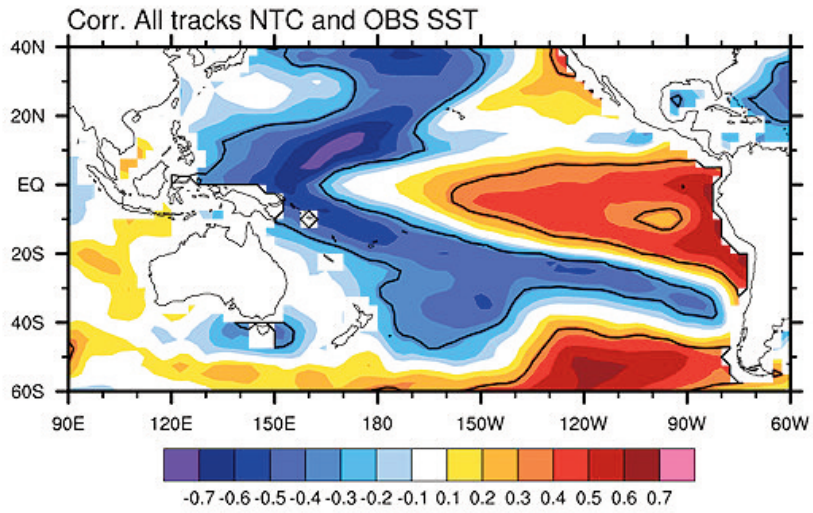

Figure 24. Spatial distribution of contemporaneous correlation coefficients between the number of TCs in the whole South Pacific and observed SST in November-April from 1983/1984 to 2008/2009. Black solid lines indicate the correlation coefficients above the 5% significance level.

Figure 25 further elaborates the relationships between the number of TCs in each cluster and the observed SST. Considering the cyclogenesis in the region covering cluster A, the variations in TC genesis with different ENSO phases are apparent in Figure 25a. Cyclogenesis in cluster A is related to the warm phase of ENSO because of increased eastward convection. Chand and Walsh (2009) note that TC genesis is enhanced east of the dateline during El Niño years, with the highest TC density centered around 10°S, 180°E. In La Niña years, the genesis positions have maximum density centered around 15°S, 170°E. They also show that the TC tracks in the FST region are separated into three clusters that exhibit distinct characteristics associated with different ENSO phases. Based on the results in Figure 25, it is well established that the ENSO phenomenon influences the annual number of TCs in the South Pacific, and therefore the SST variation with ENSO phases can be considered to be one of the potential predictors.

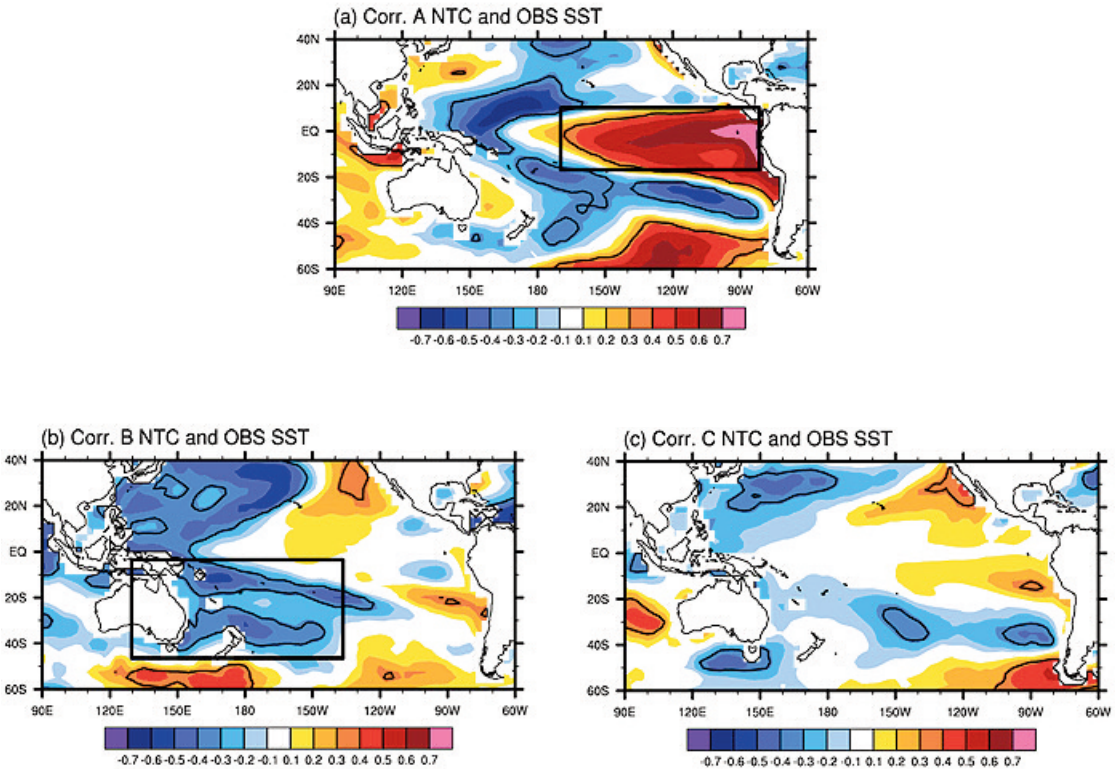

Figure 25. Spatial distribution of contemporaneous correlation coefficients between the number of TCs in each cluster in the South Pacific and observed SST in November-April from 1983/1984 to 2008/2009. Black solid lines indicate the correlation coefficients above the 5% significance level. Boxes indicate the regions where SSTs are averaged and used as predictors for the dynamical-statistical forecasts of TC activity for each cluster in the South Pacific Ocean.

Weak to moderate VWS is one of the major atmospheric parameters favorable for TC development. The VWS disturbances have been found to be influenced by fluctuations in SST. Dowdy et al. (2012) found that negative (positive) departures of VWS dominate the northern regions of the South Pacific Ocean during El Niño (La Niña) years, while negative (positive) departures are located to the south. Evans and Allen (1992) explored the link between ENSO extremes, the Australian monsoon trough, and associated TC activity using observation data. Significant differences in the structure of the monsoon trough and associated TC activity were linked to the ENSO phases.

Figure 26 demonstrates the relationships between the annual variations of the number of TCs in each cluster and the observed VWS. It shows that the seasonal TC number in each cluster in the South Pacific is strongly related to the decreasing VWS in the central and eastern Pacific during the November-April TC season. Therefore, the VWS variations as potential predictors come from the signals in the central Pacific, which is modulated by ENSO (Figure 26a). Figure 26b-c also show that the number of TCs in cluster B and C is related to the decreasing VWS in the eastern or central Pacific, but the magnitude of the relationship is much weaker than that of cluster A.

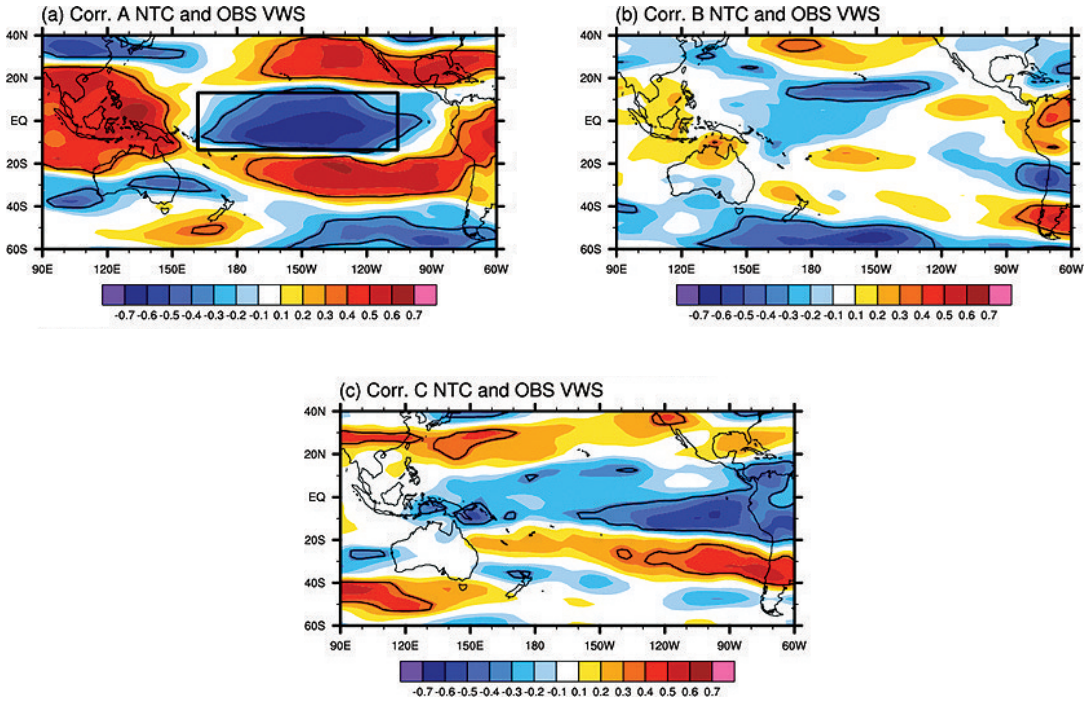

Figure 26. Spatial distribution of contemporaneous correlation coefficients between the number of TCs in each cluster in the South Pacific and observed VWS during November-April from 1983/1984 to 2008/2009. Black solid lines indicate the correlation coefficients above the 5% significance level. Boxes indicate the regions where VWSs are averaged and used as predictors for the dynamical-statistical forecasts of TC activity for each cluster in the South Pacific Ocean.

The seasonal frequency of TCs in each cluster is strongly related to the observed low-level vorticity. Figure 27 shows that the seasonal number of TCs in each cluster in the South Pacific is strongly related to the local cyclonic vorticity. In contrast to the thermo-dynamical variables (e.g., SST), vorticity is found to have a strong local correlation with the annual number of TC genesis for the November-April cyclone season. The annual variability of TCs in cluster A has a more recognizable relationship with VOR (Figure 27a), but those in cluster B and C have little connection to the cyclonic vorticity in the entire Pacific (Figure 27b-c). Compared to the relationship in clusters B and C, the annual variability of TCs in cluster A has a strong correlation with anticy clonic (and cyclonic) vorticity in the central Pacific (boxed areas in Figure 27a). In those areas, the variations of low-level relative vorticity and upper-level divergence are associated with each phase of ENSO (e.g., Chand and Walsh 2009).

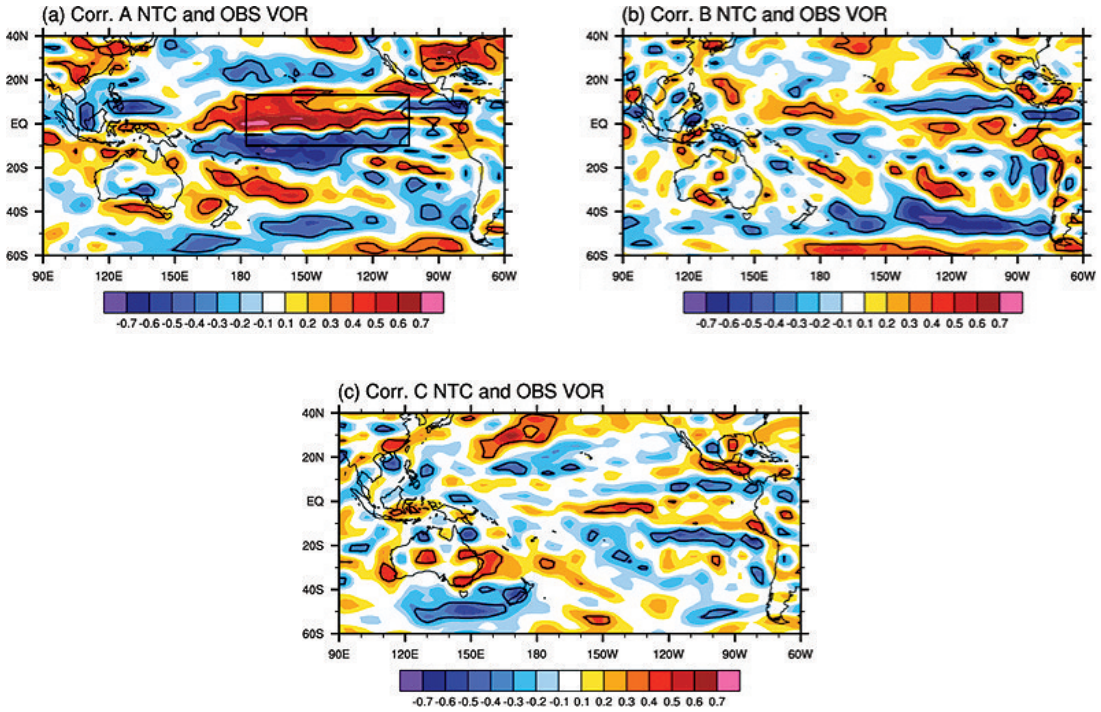

Figure 27. Spatial distribution of contemporaneous correlation coefficients between the number of TCs in each cluster in the South Pacific and observed VOR during November-April from 1983/1984 to 2008/2009. Black solid lines indicate the correlation coefficients above the 5% significance level. Boxes indicate the regions where VORs are averaged and used as predictors for the dynamical-statistical forecasts of TC activity for each cluster in the South Pacific Ocean.

The pattern of 500 hPa geopotential height (GPH) can provide limited but useful information about the environment's favorability for TC development in the South Pacific. With regards to TC genesis in cluster B, the GPH pattern represents a strong negative correlation pattern throughout subtropical central South Pacific (Figure 28b). The APCC MME represents the significant spatial correlation distribution between the interannual variability of TCs in cluster B and the GPH hindcasts, which is comparable to the observations. Therefore, the GPH in the subtropical South Pacific (the boxed region in Figure 28b) is selected as one of the predictors for the TC number in cluster B. The TC genesis within the area for cluster C is generally from the cross-equatorial flow from the Northern Hemisphere associated with cold surges from Asia. In fact, we can see an observed significant negative correlation (60°E-150°E, 20°N-40°N) in Figure 28c, which is consistent with the simulated negative correlation. Therefore, we also include the GPH within the area (boxed region in Figure 28c) as an additional predictor for the TC number in cluster C.

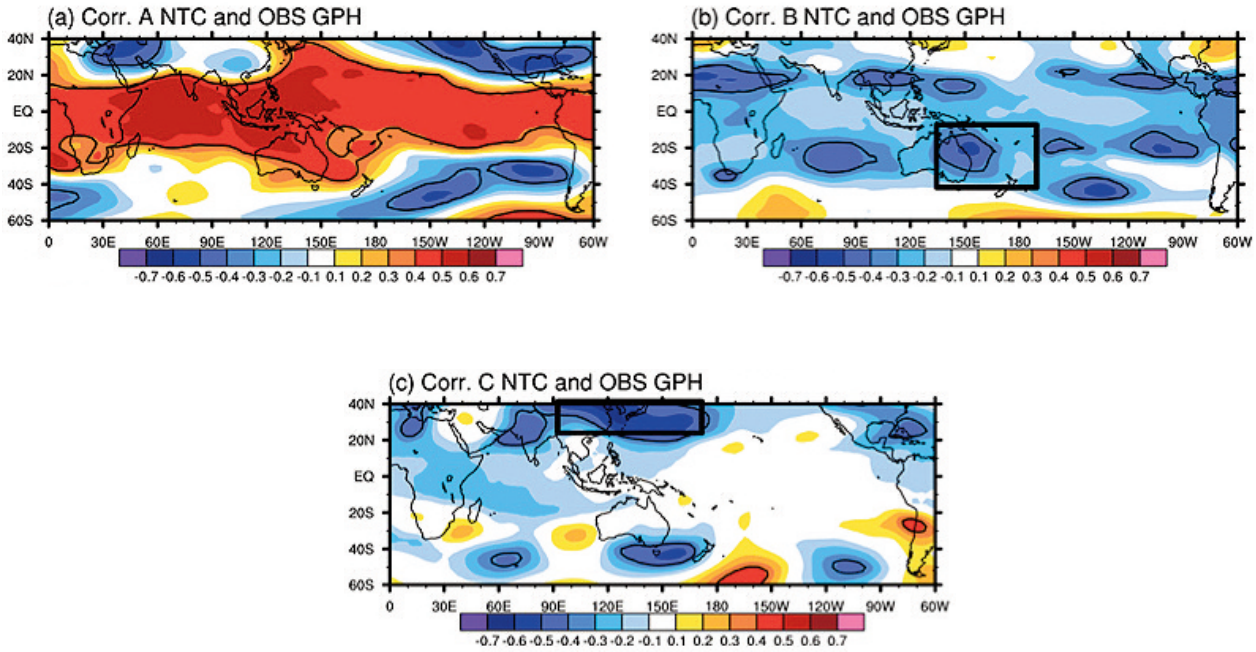

Figure 28. Spatial distribution of contemporaneous correlation coefficients between the number of TCs in each cluster in the South Pacific and observed GPH during November-April from 1983/1984 to 2008/2009. Black solid lines indicate the correlation coefficients above the 5% significance level. Boxes indicate the regions where GPHs are averaged and used as predictors for the dynamical-statistical forecasts of TC activity for each cluster in the South Pacific Ocean.

As revealed in Figure 25 through Figure 28, the TC number in cluster C shows less of a correlation to the observed- and MME-predicted large-scale fields, and thus there were no predictors selected with simultaneous relationships with the TC number for cluster C. Instead, observed fields in the preseason can be considered to be meaningful potential predictors based on a lagged relationship. Werner and Holbrook (2011) found that meridional winds at 850 hPa (V850) and SST prior to the TC season produces higher skills for predicting tropical cyclogenesis. We realized that the correlation pattern of V850 north of the equator in the far eastern Pacific has a statistically significant negative relationship with TC number in cluster C (Figure 29a). The regression map of SST in the pre-TC season onto the TC number in cluster C, demonstrates pre-TC season SST are char acterized by the developing ENSO pattern, and thus SST in the central equatorial Pacific could serve as an indicator for cyclogenesis in cluster C (Figure 29b).

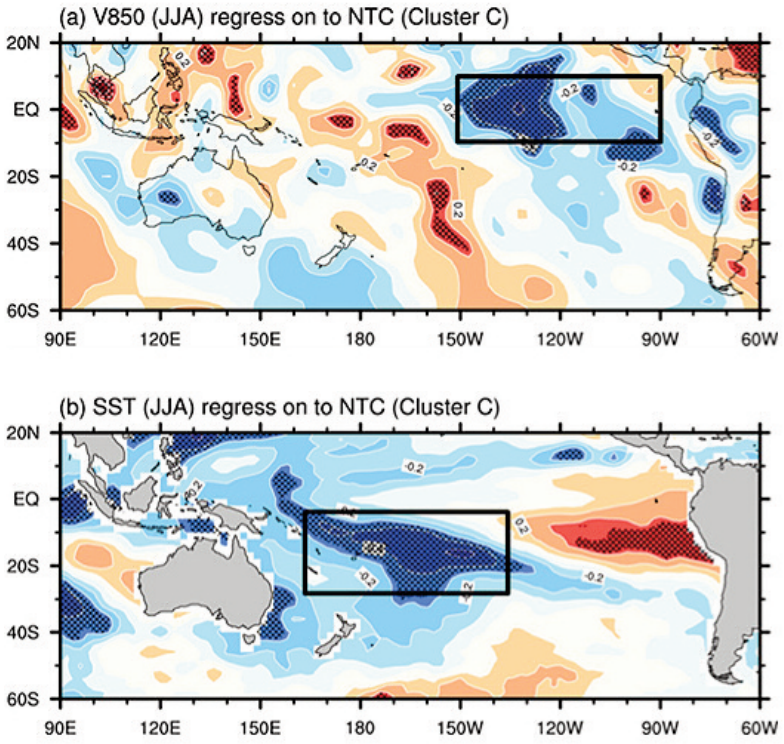

Figure 29. Regression map of (a) V850 and (b) SST in JJA onto the number of TCs during November-April in cluster C. The regions marked by a crisscross pattern indicate that the correlation coefficients above the 5% significance level. Boxes indicate the regions where V850 and SST are averaged and used as predictors for the dynamical-statistical of TC activity for cluster C.

A common way of verifying prediction methods is to use cross-validation. Because the interannual variation of seasonal TC frequency in each cluster is almost independent from year to year, it is suitable to use the leave -one-out cross-validation method. For the first step, we implement a simple (one predictor only) or multiple (multiple predictors) regression analysis between the selected predictors and predictand for each TC track cluster over the whole hindcast period, except for the target year. Then, the regression coefficients are applied to the APCC MME forecast for the target year for each cluster to yield the predicted TC frequencies in each cluster.

Figure 30 shows the hindcasts for the TC number for the period of 1982/1983-2008/2009 using the hybrid prediction model. The hindcasts predict the general fluctuations of TCs in accordance with the actual number of observed TCs in cluster A (Figure 30a). In particular, the MME hindcasts capture the interannual variation influenced by the different phases of ENSO in the cluster. For example, the hindcasts reasonably represent the several observed major active TC seasons in cluster A in 1986/1987, 1991/1992, 1992/1993, 1997/1998, 2002/2003, 2004/2005, and 2006/2007, which is consistent with the major warm phases of ENSO episodes.

Contrary to cluster A, significant errors are found in many years in clusters B and C. In these clusters, the prediction of seasonal TC frequency cannot capture the observed year-to-year fluctuation of seasonal TC numbers. This is can be attributed somewhat to the weaker relationship between the seasonal TC number in those clusters and simultaneous large-scale environmental fields. Further research is needed to improve the prediction of the seasonal TC number for clusters B and C, and should include the identification of appropriate predictors for the statistical-dynamical models.

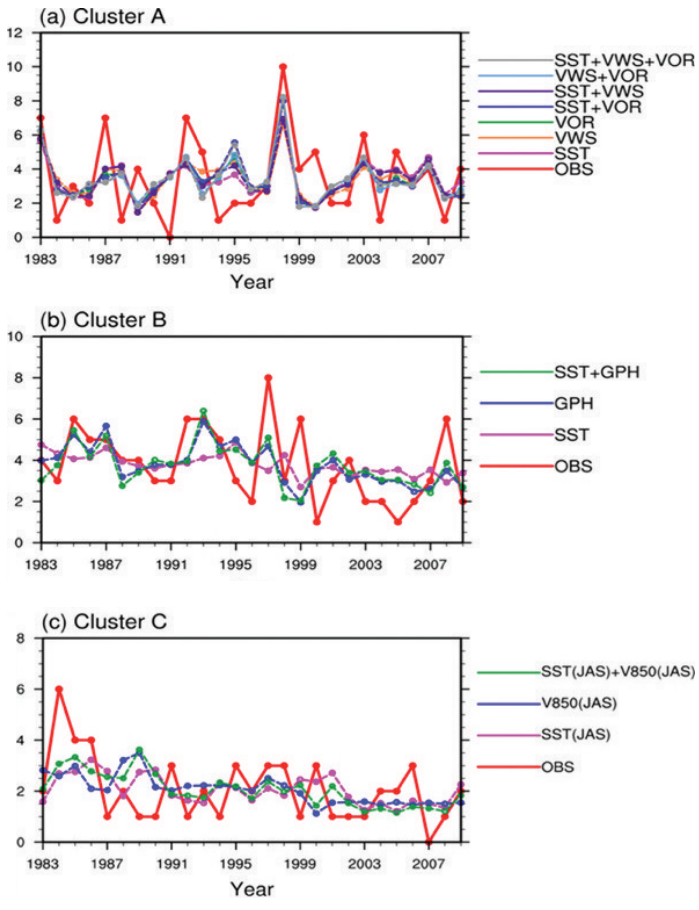

Figure 30. Observed (thick red lines with closed circles) and predicted number of TCs in each cluster. All forecasts are 1-yr-out cross-validated.

All of the predictors can partially explain the interannual variation of TC number in the South Pacific. However, the inclusion of many potential predictors in the multivariate regression does not necessarily guarantee better predictability, due to the overfitting problem (Wilks 2006). The potential predictors selected in the previous section are indeed mutually correlated and dependent on one another through large-scale circulation changes associated with ENSO. In this study, we select the best set of predictor variables from the potential predictors. Table 6 summarizes the statistical measures between the observed and predicted number of TCs for each cluster, in which the prediction is made by using predictors individually or in combination. The measures include correlation coefficient (CORR), root mean squared errors (RMSE), and mean square skill scores (MSSS). The MSSS represents the ratio between the reduction in the MSE of the model predictions and the MSE from the climatology references. From Table 6, we select VOR as the best predictor for cluster A, for the largest COR, the smallest RMSE, and the largest MSSS. The selection method is the same for each cluster, while the selected predictors are different for each cluster. Of the three potential predictors, one or two are selected for each cluster.

Table 6. Correlation coefficients (CORR), root mean squared errors (RMSE), and mean square skill scores (MSSS) between observed and predicted number of TCs in each cluster. Numbers in bold indicate the predictor combination that was finally chosen to be the best predictor(s).

Cluster	Predictors	CORR	RMSE	MSSS
A	SST+VWS+VOR	0.53	2.01	0.27
	SST+VWS	0.49	2.06	0.24
	SST+VOR	0.57	1.95	0.32
	VWS+VOR	0.57	1.94	0.33
	SST	0.55	1.99	0.29
	VWS	0.53	2.01	0.28
	VOR	**0.61**	**1.88**	**0.36**
B	**SST+GPH**	**0.48**	**1.80**	**-0.01**
	SST	0.04	1.56	0.20
	GPH	0.46	1.30	-0.04
C	GPH	0.08	1.30	-0.04
	SST(JJA)	0.29	1.23	0.06
	V850(JJA)	0.23	1.27	0.00
	SST(JJA)+V850(JJA)	**0.34**	**1.22**	**0.08**
	GPH+SST(JJA)+V850(JJA)	0.22	1.30	-0.04

We perform the validation for year-to-year TC track density anomalies of the cross-validated forecasts from APCC MME hindcasts from 1982/1983 to 2008/2009. The validation includes the quantitative skill scores, such as accuracy (ACC), Heidke skill score (HSS), and Hanssen and Kuipers discriminant (HK) (Wilks 2006). This validation is based on a contingency table for multi-category (3x3) forecasts.

The APCC MME-statistical based TC prediction shows a higher level of accuracy near and west of the dateline, but a rather lower level of accuracy far east of the dateline. The APCC model is well above 0.6 near and west of the dateline (Figure 31a). The HSS and HK (Figure 31b-c) in those regions range from 0.2 to 0.3 or higher, indicating higher accuracy in those regions. In some areas in the far eastern Pacific, however, the score is close to 0, implying that it would be better to use climatology. In conclusion, the prediction model developed in this study shows higher skills in the region where there is climatologically higher TC track density.

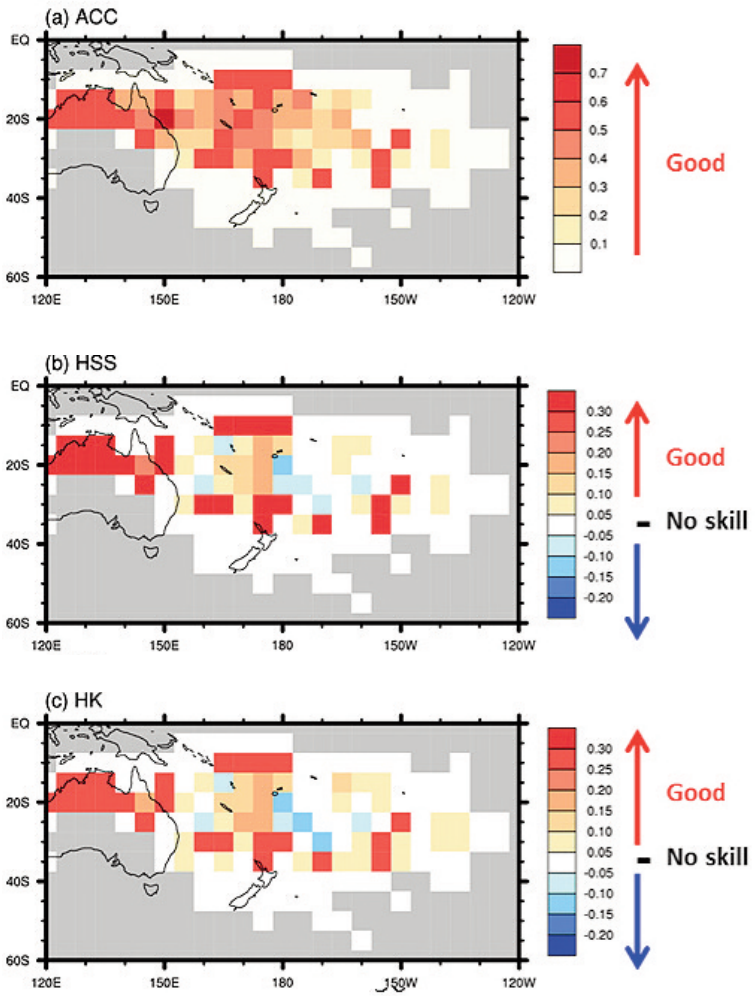

Figure 31. Skill scores for the seasonal TC track density anomalies predicted from APCC MME hindcast from 1982/1983 to 2008/2009: (a) ACC, (b) Heidke skill score, and (c) Hanssen and Kuipers discriminant.

We issued seasonal TC forecasting for 2016/2017 using the hybrid statistical-dynamical model developed in this study. Figure 32 shows the TC track density map for 2016/2017 and its anomaly compared to the climatological TC occurrence distribution. The model predicts the highest TC track density in the area near 160°E-180°E and 15°S-20°S. The TC track density anomaly, on the other hand, shows near-normal TC track probability near and east of the dateline compared to the climatological distribution, but a bit lower TC track probability west of the dateline. Thus, for countries near and east of the dateline, there would be a chance of TC occurrence near the climatological average. For countries near Coral Sea and west of dateline, there would be a chance of below-normal TC occurrence.

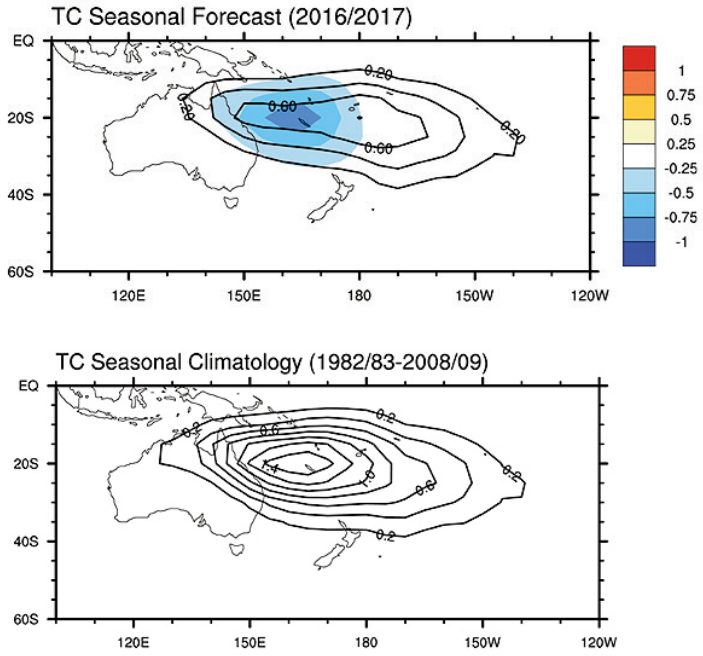

Figure 32. (a) Seasonal TC forecast track density (contour) and its anomaly compared to the climatological TC track density (shaded) during NDJFMA in 2016/2017 from the hybrid statistical-dynamical model based on APCC MME forecasts, (b) Climatological TC track density over 1982/1983 to 2008/2009.

The seasonal TC activity prediction from the APCC MME forecast is then compared to the forecasts from other agencies, including the Bureau of Meteorology (BoM), Australia, and the regional specialized meteorological center-Nadi (RSMC-Nadi). At BoM, the outlook is produced using statistical relationships between tropical cyclone numbers and two indicators: the Southern Oscillation Index (SOI) and the Niño-3.4 SST index (Figure 33). In the BoM outlook, neutral to weak La Niña conditions in the tropical Pacific Ocean increases the odds of the above-average number of tropical cyclones for the western South Pacific region. The outlook also states that near-average cyclone numbers are likely for the eastern South Pacific, but that the model accuracy is very low. The South Pacific tropical cyclone season experiences most of its cyclones between 1 November and 30 April and averages around seven tropical cyclones in the western region and ten in the eastern region. Tropical cyclones impact Pacific Island countries during most years, and coastal impacts can be felt even when tropical cyclones remain well offshore.

At RSMC-Nadi, the outlook is produced based on the analogue method in which an analogue of six seasons (1978/1979, 1981/82, 1985/1986, 1989/1990, 2013/14) with similar atmospheric and oceanic condition is used to produce this year's outlook (Figure 34). In their outlook, five to seven (5 to 7) tropical cyclones are expected to occur in the RSMC Nadi-TCC AoR during the 2016/17 season. The average for all of the 47 seasons from 1969-70 to 2015-16 is 7.3 cyclones. The average for El Niño, La Niña, and neutral seasons are 8.7, 6.5, and 6.4 cyclones, respectively. Tropical cyclone genesis trough is expected to be shifted to the west of the dateline during the 2016/17 season. This outlook is based on the status of the El Niño Southern Oscillation (ENSO) over the preceding July to September period. During this period in 2016, neutral to weak La Niña conditions were present and the International Climate Model Guidance indicates that the most likely outcome for the 2016/17 season is for neutral conditions to prevail. Therefore the seasonal outlook is based on weak La Niña to neutral conditions. Historically, these conditions have favored a westward shift in tropical cyclone activity in the Southwest Pacific.

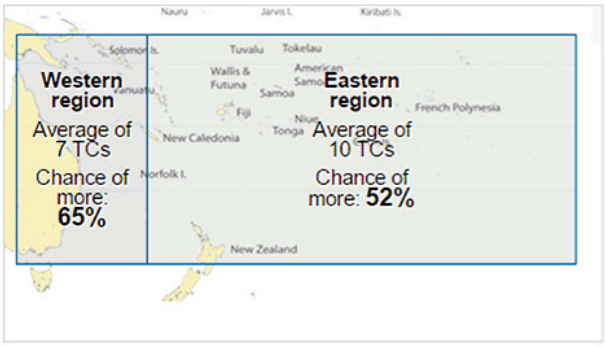

Region	Long-term* average number of tropical cyclones	Chance of more tropical cyclones
Western	7	65%
Eastern	10	52%

The long-term average number of tropical cyclones is calculated using data from the 1969–70 season up to this (2016) season.

Figure 33. South Pacific seasonal tropical cyclone outlook for 2016/2017 from the Bureau of Meteorology, Australia (http://www.bom.gov.au/climate/cyclones/south-pacific/archive/20161014.archive.shtml).

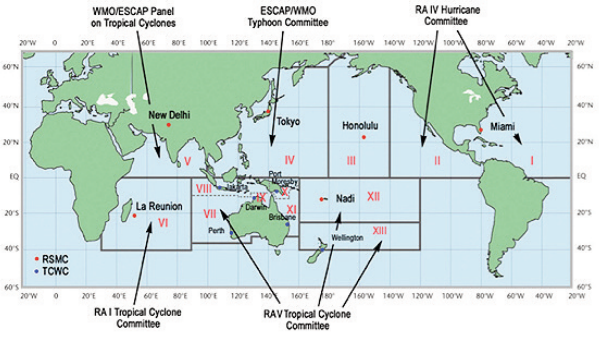

Figure 34. Tropical cyclone seasonal outlook for 2016/2017 in the RSMC-Nadi tropical cyclone center area of responsibility (http://www.met.gov.fj/aifs_prods/2016-17_Tropical_Cyclone_Outlook.pdf).

Seasons	TC Occurrence (RCMC-TCC Nadi Aor)	Severe TC(Cat 3-5) (Rsmc-TCC Nadi Aor)
1978/79	6	3
1981/82	6	5
1985/86	7	3
1989/90	7	3
2008/09	5	0
2013/14	6	2
Average(Median)	6.2(6)	2.7(3)

4.2 Subseasonal Tropical Cyclone Forecast

— Accurate predictions of tropical cyclones (TCs) can benefit emergency preparedness and disaster mit igation in many coastal regions in the South Pacific. As short lead-time forecasts and high-resolution numerical weather prediction models can provide accurate forecasts of the genesis and tracks of individual TCs out to approximately five days (WMO 2014). However, beyond this time scale, the nature of the atmosphere makes it impossible to forecast individual TCs, and instead TC activity statistics, such as their genesis or frequency, are predicted. With the improvement in seasonal climate prediction, more attention has been given to successful seasonal TC activity forecasts in various basins. However, rela tively little effort has been given to the prediction of TC activity on the sub-seasonal time scales. Motivated by this framework, the ultimate aim of this research is to provide reliable probabilistic information on TC occurrences in the South Pacific during week-long periods.

The tropical outlook is an official product of the National Oceanic and Atmospheric Administration (NOAA) Climate Prediction Center (CPC), which includes regions where tropical cyclogenesis is favored for the upcoming week-1 and week-2 time periods . Tropical cyclone areas from the outlook are subjectively created based on various objective forecast tools, such as Madden-Julian oscillation (MJO) composites, statistical and dynamical tropical cyclone forecasts, and raw model forecast guidance. Paul Roundy forecasts experimentally provide prob ability TC forecasts and anomalies, which are based on seasonal and 100-day low-pass patterns and/or MJO patterns. The European Centre for Medium-range Weather Forecasts (ECMWF) employs 32-day Ensemble Prediction System (EPS) for weekly mean tropical cyclone strike probability. Leroy and Wheeler (2008) also developed a purely statistical prediction system with several predictors based on seasonal tropical cyclone activity in the South Pacific. Even though both statistical and dynamical methods are capable of predicting sub-seasonal TC activity during several weeks, the hybrid dynamical-statistical model potentially improves accuracy for sub-seasonal TC activity forecasts beyond that of the component models. In a hybrid dynamical-statistical model, dynamic model-based predictions of large-scale variables can be used as a set of predictors for forecasting the statistical TC activity (e.g., occurrence) during several upcoming weeks. Therefore, the ultimate aims of this study are to provide reliable probabilistic information on sub-seasonal TC occurrence forecasts in the South Pacific through a hybrid dynamical-statistical model.

For a successful sub-seasonal TC activity forecast, it is important that we identify possible indicators of sub-seasonal predictability for South Pacific tropical cyclones and demonstrate model capabilities. Sub-seasonal variations in tropical convective activity play a significant role in the coupled atmosphere-ocean system and MJO is the strongest mode of tropical sub-seasonal atmospheric variability (Madden and Julian 1994). Many previous studies have demonstrated both an extended-range predictability of MJO out to about 20 days (e.g., Waliser et al. 1999; Lo and Hendon 2000), and the existence of a strong contemporaneous relationship between MJO and TC activity (e.g., Maloney and Hartmann 2000; Hall et al. 2001). In combination, these two pieces of evidence support using MJO as one of the potential predictors of weekly TC activity, which is outlined in this work.

Several statistical models have been developed for MJO predictions based on various statistical methods, such as a regression using an empirical orthogonal function (EOF; Jones et al. 2004; Jiang et al. 2008), singular spectrum analysis (Mo 2001), and wavelet analysis (Webster and Hoyos 2004). Kand and Kim (2010) compared the performance of

1. http://www.cpc.ncep.noaa.gov/products/precip/CWlink/ghazards/index.php
2. http://www.atmos.albany.edu/facstaff/roundy/tcforecast/tcforecast.html

these statistical models in simulating MJO and indicated that the multi-regression method shows the best skill. Jiang et al. (2008) and Jones et al. (2004) demonstrated that the multi-regression model has an MJO predictability with the time scale of a few weeks. Dynamical models are applicable to MJO forecasts, which have some usefulness in predicting the MJO for some seasons compared to statistical models (e.g., Seo et al. 2009; Kang and Kim 2010; Matsueda and Endo 2011; Lin et al. 2008; Gottschalck et al. 2010). In particular, Matsueda and Endo (2011) demonstrated that operational medium-range ensemble forecasts, available at The Observing system Research and Predictability Experiment (THORPEX) Interactive Grand Global Ensemble (TIGGE) data portal, perform well in simulating the maintenance and onset of MJO in some phases.

In addition to MJO, there are other possible indicators of sub-seasonal prediction of South Pacific TC activity. The physical basis for TC activity prediction depends on information indicating that the large-scale environment favors TC genesis. Frank (1987) documented the necessary conditions for TC genesis: (1) warm local sea surface temperatures coupled with a relatively deep oceanic mixed layer, (2) large cyclonic absolute vorticity in the lower troposphere, (3) weak vertical wind shear over the pre-storm disturbance, and (4) high mid-level humidity. The key to TC activity prediction is identifying physically meaningful and predictable phenomena that affect conditions related to TC activity. Therefore, we consider likely and/or possible potential predictors in addition to MJO for weekly TC activity predictions. Possible predictors include SST variability in the Indo-Pacific associated with ENSO, interannual variability associated with SST (local SST) (Leroy and Wheeler 2008), and low-level relative vorticity anomalies (Hall et al. 2001). Vincent et al. (2009) also studied the location of the South Pacific Convergence Zone (SPCZ) as a strong modulator of atmospheric circulation variability in the South Pacific, and accordingly generating TCs. With careful investigation and selection of the aforementioned predictors, a prediction model was developed to predict the probability of TC occurrence in the South Pacific during upcoming weeks. Note that predictors used in real-time forecasting of TC occurrence in the hybrid model have to be uncorrelated, available in real-time, and without their own trend.

The Observing system Research and Predictability Experiment (THORPEX) is a 10-year international research program organized by the World Meteorological Organization (WMO) with the purpose of improving the accuracy of one-day to two-week forecasts of severe weather events for societal, economical, and environmental benefits (WMO 2005). Since October 2006, THORPEX has provided 10 global ensemble forecast datasets through TIGGE data portals (Bougeault et al. 2010). Using TIGGE is an effective mechanism for rapidly identifying severe weather events, such as tropical and extratropical cyclones, the MJO, and heavy rainfall and floods, and related phenomena. Although ensemble forecast data are available from several NWP centers, the forecast data used in this study are obtained from operational medium-range ensemble forecasts from one of the leading global NWP centers, ECMWF.

The ensembles for outgoing longwave radiation (OLR) and 850 hPa and 200 hPa horizontal winds (U850 and U200) are obtained from the TIGGE portal at ECMWF (http://tigge.ecmwf.int) and are available with a two-day delay as part of the THORPEX research program for non-commercial research purposes only. The ECMWF ensemble forecast consists of 50 perturbation runs as well as one control run, and provides 15-day forecasts. This study analyzes the ensemble forecasts initialized at 00 UTC from November 1, 2006 to April 30, 2015. The forecast data are interpolated to a common grid spacing of 2.5° (latitude) by 2.5° (longitude).

Several previous studies have investigated the predictability of TIGGE in terms of diverse atmospheric events. Su et al. (2014) evaluated TIGGE ensemble predictions for extreme summer precipitation. They showed that ECMWF generally performs best, while the CMC is relatively good for short-range (proba bilistic) quantitative precipitation forecasts at light precipitation thresholds. Froude (2010, 2011) com pared TIGGE predictions for extratropical cyclones using different ensemble prediction systems. In these studies, the ECMWF ensemble mean and control have the highest level of skill for all cyclone properties (e.g., cycle position, intensity, and prop agation speed). However, JMA, NCEP, UKMO, and CMC have one-day less skill for cyclone position throughout the forecast range. In addition, the relative performance of the different ensemble pre diction systems remains broadly consistent between the two hemispheres.

Before discussing the modulation of TC genesis, it is relevant to understand the characteristic framework in which TCs and large-scale waves occur. It is also useful to know the seasonal and geographical distribution of the recorded TC forma tions in the target region. Figure 35 shows the monthly climate variation of TC occurrences from 1982/83 to 2013/14, which were calculated using TCs recorded by the Joint Typhoon Warning Center (JTWC). The number of TCs in each month indicates that most TCs occurred between November and April each year. In particular, January-March is the main period for TC occurrence in the South Pacific. TC occurrence is primarily concentrated west of the dateline, but TC's also occur between 10°S-20°S throughout the South Pacific Ocean. Therefore, it is important to define the target zones of interest to develop weekly TC forecast models.

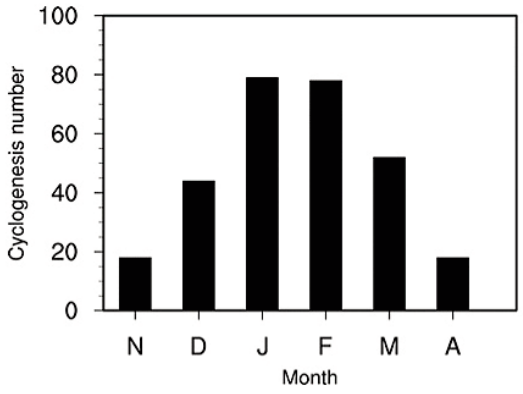

Figure 35. Monthly climate variation of TC occurrence in the South Pacific Ocean from 1982/1983 to 2013/2014 (32 years).

The formation and life cycle of TCs are associated with thermodynamic and dynamic conditions of the large-scale environment. Focusing on the dynamical aspects of the basic-state flow, the mean lower and upper-level wind fields for the austral summer (November-April) are displayed in Figure 36. In the upper level (Figure 36a), the 200 hPa streamline indicates the occurrence of westerlies poleward of 20°S, easterlies north of 10°S, and recurving flow in between. In the lower level (Figure 36b), 850 hPa streamlines show the anticyclone, centered on 30°S, 170°W. Cross-equatorial monsoon flows are present between the 0°-5°S latitudes, with the monsoon trough indicated by cyclonically recurving flow. Overall, Figure 36 indicates that the geographical position of TC genesis is located just poleward of the low-level monsoon trough and is collocated with the recurving flow in the upper level. Consistent with previous studies, weak vertical wind shear and large cyclonic vorticity are favorable for TC genesis in the South Pacific Ocean.

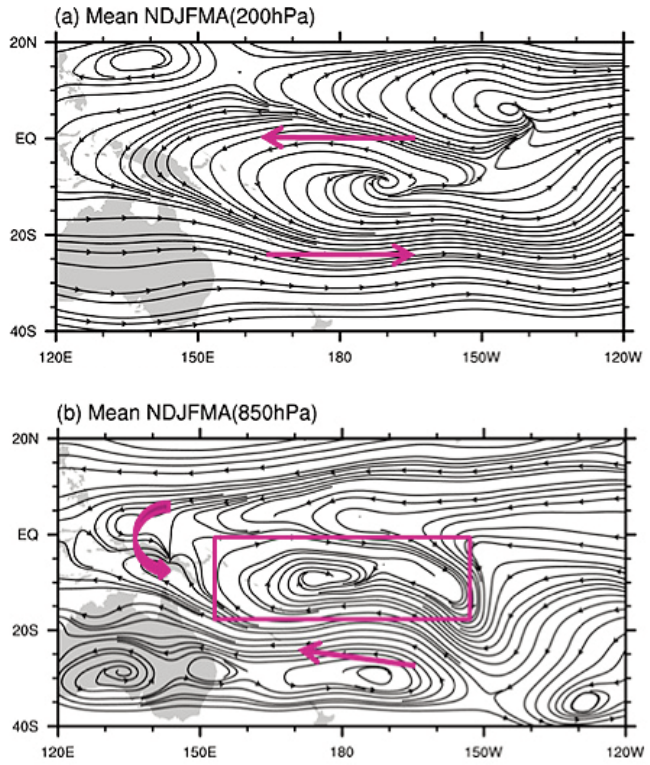

Figure 36. Austral summer (November-April) mean streamlines at the (a) 200 hPa and (b) 850 hPa levels.

The TC forecast model is developed in three different zones, as shown in Figure 37. The selection of these zones is based on physical consideration of TC activity in the South Pacific Ocean. The TCs that occur west of the boundary at 150°E have mean westward trajectories, whereas TCs that occur east of 150°E have mean eastward movement. The 180°E boundary (dateline) approximately separates regions that are well known to have contrasting responses to ENSO. Latitudinal boundaries are set at 0°S to 30°S.

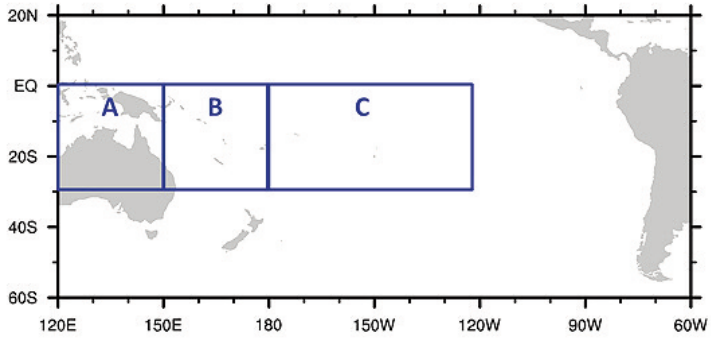

Figure 37. Three selected zones; a sub-seasonal TC occurrence prediction model was developed for each zone.

Figure 38 demonstrates the seasonal climate cycle for weekly TC genesis probabilities (black histograms in Figure 38) from 2006 to 2015. Probabilities refer to TC genesis in the week starting on each day in a year. It is clear that the probability of TC genesis during a week in January and February (i.e., the peak TC season) is much higher than in other months, indicating apparent seasonality of weekly TC probabilities. Due to the small sample size for averaging TCs, the raw climatological probabilities computed from daily data are noisy. Therefore, the raw probabilities are smoothed using Fourier analysis applied to the 365-day climate record reconstructed with the mean and first annual harmonics (red lines in Figure 38). The first harmonics account for about 40% of total variance and the second and higher harmonics have very small amplitudes compared to that of the first. As shown in Figure 38, the smoothed probabilities seem to more accurately reflect the real seasonal cycle of TC genesis. We use smoothed probabilities for seasonal climate cycles of weekly TC genesis hereafter.

To further verify the use of smoothing functions shown in Figure 38, the climatological monthly variation of TC occurrences from 1982/83 to 2013/14 is presented. The seasonal TC cycle for each region indicates that the first harmonics fitting functions are reasonable enough for weekly TC probabilities representations

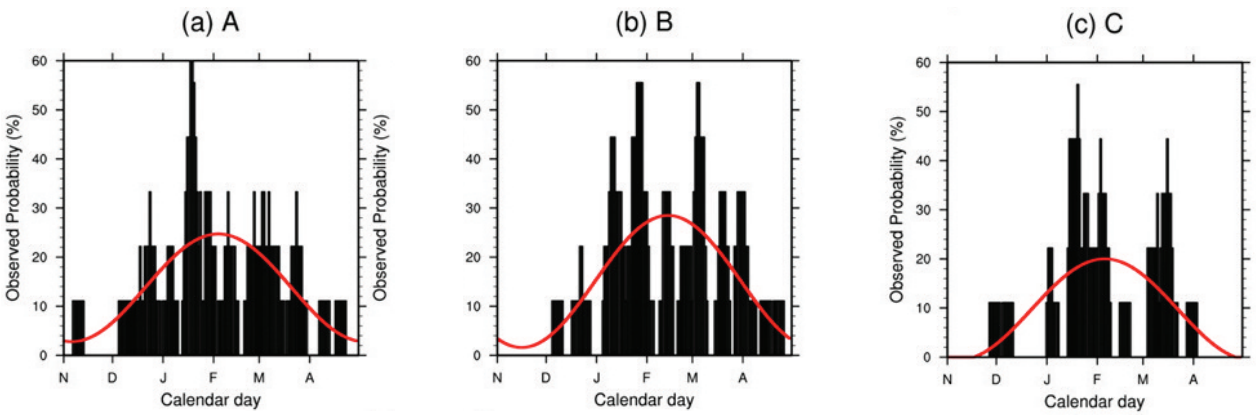

Figure 38. Seasonal climate cycles of weekly TC genesis probabilities for each zone shown in Figure 37. Probabilities (black his togram) refer to the probability of TC genesis in the week starting every day during the active TC season from Sep tember to August. The red curves denote the weekly TC genesis cycle smoothed using Fourier analysis applied to the 365-day climatology and reconstructed using only the mean and the first annual harmonics.

As mentioned earlier, the contemporaneous relationships between the RMM-based MJO phase and TC genesis in the South Pacific were well-established in several previous studies. Leroy and Wheeler (2008) binned TC genesis locations according to predefined MJO phase categories. They found that the TC genesis peaked in phases 4, 5, 6, and 7 near Australia, and phases 6, 7, 8, and 1 for the South Pacific based on TC data for the years 1969-2004. Ramsay et al. (2012) conducted a cluster analysis of TC activity in the Southern Hemisphere and found that TC activity in the South Pacific is favored when the MJO-enhanced convection is located over the western Pacific and Western Hemisphere.

The simultaneous relationship between the observed MJO index and TC genesis is demonstrated by binning the TC genesis locations for each MJO phase category (Figure 39). In Figure 39, the role of the MJO in modulating TC genesis can be recognized. Consistent with the results of previous studies, TC genesis locations tend to be located poleward and westward of the strong MJO convection. TC genesis in northern Australia and the Coral Sea peaks in MJO phases 2, 3, 4, and 5 (Figure 39a, b). The peak of TC genesis in the South Pacific is during MJO phases 6, 7, 8, and 1, but TC genesis is less favored in MJO phases 2, 3, 4, and 5 (Figure 39c, d). In the case of weak MJO phases (Figure 39e), many TC genesis have also been found longitudinally near 10°S-20°S, implying other possible local factors that favor TC genesis. Given the extended-range predictability of the MJO from TIGGE forecasts, and the existence ofa strong contemporaneous relationship between MJO and TC occurrence, it is reasonable to use the MJO index calculated from TIGGE forecasts as two predictors for the TC forecast statistical model.

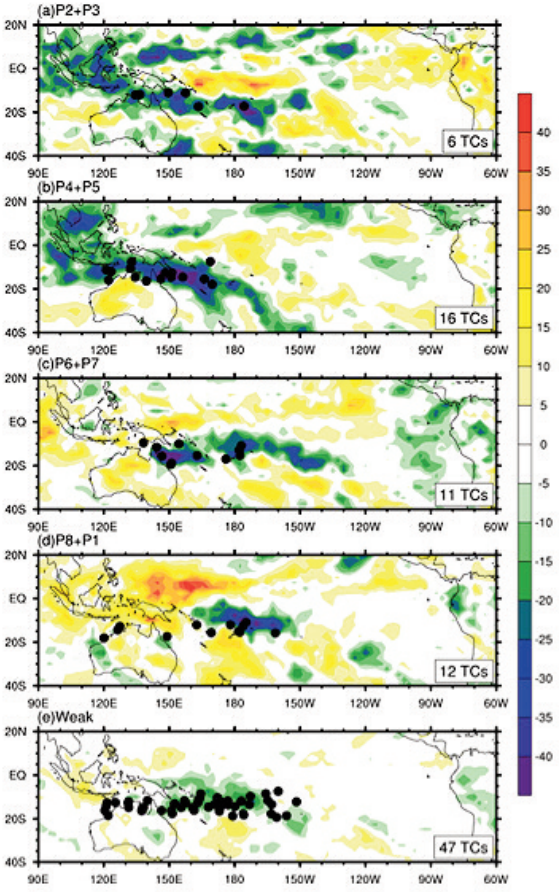

Figure 39. TC genesis locations (black dots) in each MJO phase, as defined by the RMM index. Also shown are OLR anom alies (shaded) for each averaged MJO phase. For sim plicity, we combine the two neighboring categories: (a) phases 2+3, (b) phases 4+5, (c) phases 6+7, and (d) phases 8+1. The bottom panel, (e) is the map for the weak MJO phases.

The SPCZ is characterized by low-level convergence between the northeasterly winds west of the south Pacific and the high and cooler southeasterly winds from higher latitudes ahead of high pressure systems, moving eastward from the Australia and New Zealand region (Barry and Chorley 2003). The SPCZ is more active in the austral summer and it is usually defined by the precipitation amount.

The position of the SPCZ is considered to be a good indicator of cyclogenesis geography in the South Pacific because the SPCZ reveals large-scale dynamic and thermodynamic fields over the region (Vincent et al. 2009). Moreover, the small displacement in the mean SPCZ position can have a strong influence on the generation of TCs in the South Pacific. The SPCZ is characterized by a zonal portion located over the western Pacific warm pool region and a latitudinal tilt portion along the northwest-southeast axis. The interannual variability of its western portion is influenced by a monsoon trough that affects the Indian Ocean and Australian region, with monsoon winds extending eastward to the dateline (Vincent et al. 2009). However, the interannual variability of the eastern SPCZ relies on interactions with higher latitude depressions and on the existence of a dry zone in the southeastern Pacific (Kiladis et al. 1989). The daily to weekly scale variability of spatial location is controlled by zonal dry air inflow associated with trade wind strength (Lintner and Neelin 2008). The SPCZ strength, area, and centroid latitude have a dominant seasonal cycle, whereas the SPCZ centroid longitude has a prominent intraseasonal variability due to MJO influence (Kidwell et al. 2015). Thus, the SPCZ variability is affected by various seasonal and/or intraseasonal phenomena.

TC genesis is known to be dependent on large-scale dynamic and thermodynamic fields and surface cyclonic vorticity is one variable that favors TC genesis (Grey 1979). In particular, 850 hPa relative vorticity anomalies are an excellent diagnostic of changes in the large-scale cyclogenesis patterns (Hall et al. 2001; Vincent et al. 2011). Vincent et al. (2011) found that the SPCZ is always collocated with the zero relative vorticity at low levels. However, the maximum vorticity lies 6° to the south of the SPCZ position, which is independent of its interannual variation. They also demonstrated that this structure in the SPCZ region constrains tropical cyclogenesis to occur favorably within 10° south of the SPCZ location. This is consistent with other studies indicating that the location of the SPCZ controls cyclogenesis distribution, which occurs on the poleward side of the tropical portion of the SPCZ. Figure 40 depicts the composite 850 hPa relative vorticity for all TC genesis days in NDJFMA from 2006 to 2015. Consistent with previous studies, the TC genesis location is considerably collocated with the large relative cyclonic vorticity around 10°S-20°S, especially west of the dateline. Thus, cyclonic relative vorticity related to SPCZ can be a good indicator (i.e., predictor) for weekly TC genesis forecasts in the South Pacific.

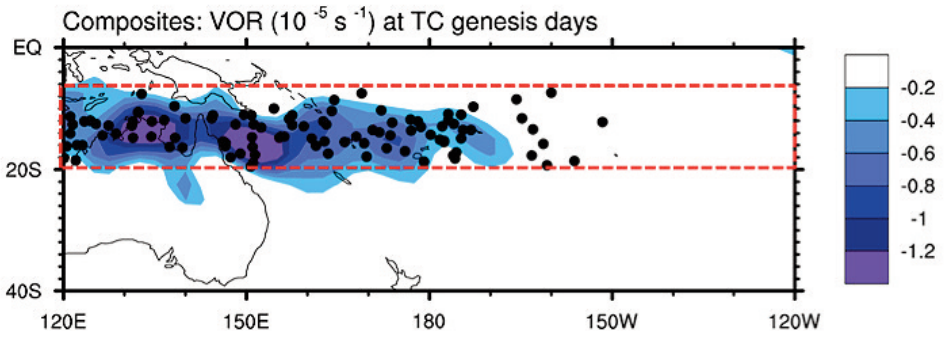

Figure 40. Shaded areas indicate mean cyclonic vorticity for all TC genesis days from 2006/11 to 2015/04. The black dots indicate the geographic locations of TC genesis.

The relationship between relative cyclonic vorticity and weekly TC genesis for each zone is further examined. Figure 41 demonstrates the seasonal cycle of relative vorticity peaks (averaged for 10°S-20°S for each zone) over a month when weekly TC genesis is the most active, especially for regions A and B (Figure 41a, b). However, the seasonal cycle of relative vorticity for region C peaks over a month earlier than that for TC genesis (Figure 41c). Thus the results in Figure 41 implies that the area-averaged relative vorticity field can be regarded as a good predictor for weekly TC genesis prediction for regions A and B, is not a good predictor for region C. Because the eastern portion of the SPCZ (for region C) is tilted along the northwest-southeast direction, the zonally averaged relative vorticity would be insufficient to be used as a TC genesis predictor for that region. There are presumably other large-scale factors that affect TC genesis for the region (e.g., ENSO). Given the collocation between the large cyclonic vorticity and TC genesis areas in regions A and B (shown in Figure 41), we employ 850 hPa relative vorticity field averaged between 10°S-20°S in each zone, instead of directly using the SPCZ characteristic (e.g., area, position, and strength).

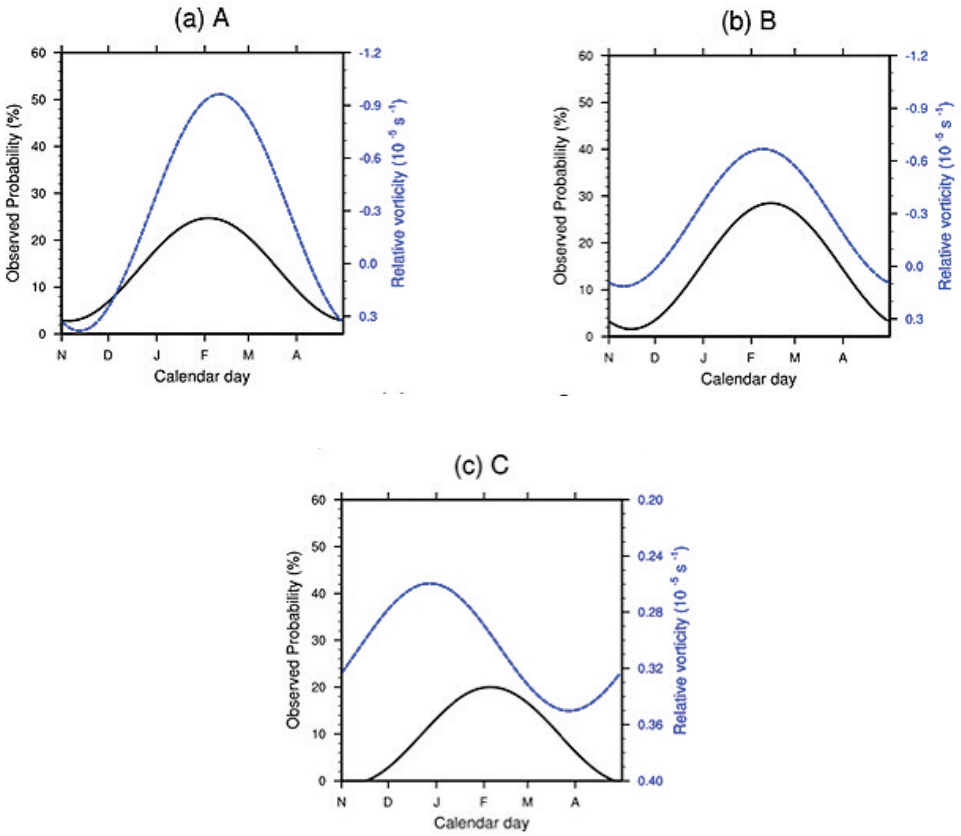

Figure 41. 22 seasonal climate cycle of TC activity (black curves) and local relative vorticity (blue curves) for each zone. Relative vorticity are averaged for the latitudes 10°S-20°S for each zone.

It is well known that the key driver of TC genesis variability in the South Pacific is ENSO. The authors have shown that the spatial patterns and characteristics of TC genesis in the South Pacific are related to the different phases of ENSO. During the positive ENSO phase, TC genesis is preferentially enhanced eastward to the South Pacific Ocean, with the highest TC density centered on the dateline. During the negative ENSO phase, TC genesis positions have their maximum density further west of the dateline, because equatorial convection moves further westwards.

Figure 42 represents the Nino3.4 index time series averaged for the TC active season (NDJFMA) from 2006/07 to 2014/15. From the time series, we select 2006/07, 2009/10, and 2014/15 as above-normal years, and 2007/08, 2010/11, and 2011/12 as below-normal years. We thus compare the simultaneous relationship between these two types of interannual SST variability and TC genesis for each zone. Figure 43 reveals that the TC genesis increases east of the dateline (region C) in the above-normal years (warm ENSO phase), consistent with previous studies. TC genesis in region A (far west of the dateline) indicates an increased TC probability in the below-normal years (cold phase of ENSO) during the TC peak season (January-February). These results are also consistent with the findings in previous studies. In region B, TC genesis probability tends to remain the same, regardless of the ENSO phase. This result implies that the Nino3.4 index, representing the behavior of ENSO, can be considered as one potential predictor for weekly TC genesis forecasts.

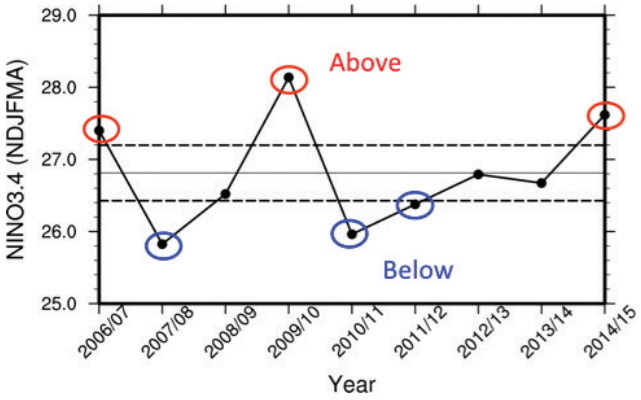

Figure 42. Time series of Nino3.4 index averaged for NDJFMA from 2006/07 to 2014/15. The gray solid line indicates the index mean during all periods, and the black dashed lines indicate the boundaries for 0.5 sigma of the index mean. From this, above-normal years are 2006/07, 2009/10, and 2014/15, and below-normal years are 2007/08, 2010/11, and 2011/12.

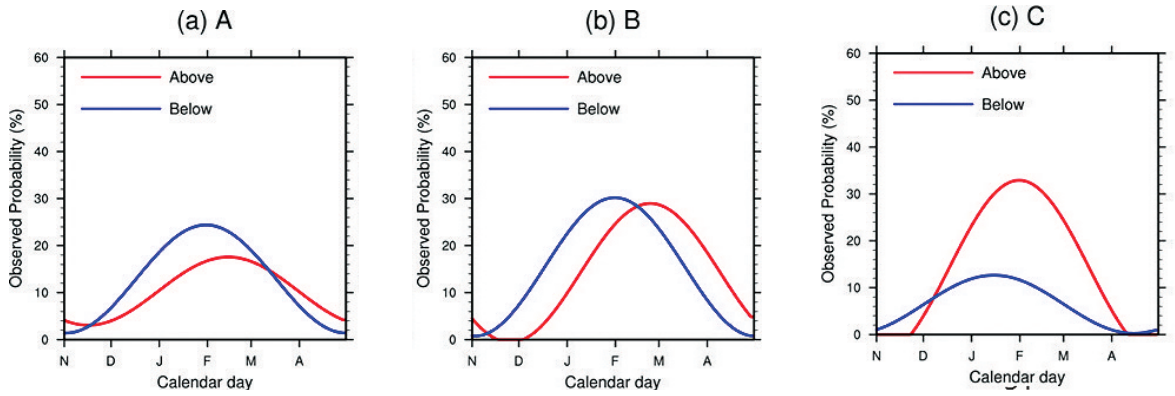

Figure 43. Seasonal climate cycle of TC activity for each zone. Above- (red) and below-normal (blue) years are defined in Figure 42. Note that above- and below-normal years correspond to warm- and cold-phase of ENSO years.

This study describes the development of a TIGGE forecast based dynamical-statistical model for predicting weekly TC genesis probability during the South Pacific Ocean active TC seasons (November-April). A distinguishing feature of this approach is that predictors are physically relevant contemporaneous seasonal large-scale environment variables derived from a dynamical TIGGE prediction. This key point is different from a pure statistical method that depends on the lag relationship with past observation records. This study identifies potential predictors associated with weekly TC genesis probability from physical consideration. In addition, the dynamical model (here, TIGGE) provides a measure of predictor accuracy.

Based on the composite analysis, consistent with the findings in previously published literature, the MJO is selected as one of the key predictors for weekly TC genesis probability. TIGGE forecasts have reasonable capability in predicting the MJO; therefore, we use MJO forecasts from TIGGE as a predictor of weekly TC genesis.

The SPCZ variation is also well known to be associated with TC genesis in the South Pacific. The large-scale conditions affecting the variability of the western and eastern SPCZ are different, and the various SPCZ characteristics (i.e., strength, area, and centroid latitude/longitude) are dominated by either seasonal or semi-annual variability. We chose to use low-level relative vorticity averaged from 10°S-20°S in each zone. Given the collocation between the large cyclonic vorticity and TC genesis areas, it is reasonable to use relative vorticity averaged in each zone instead of directly using various SPCZ characteristics. Based on our analysis, the area-averaged relative vorticity field is a good predictor for weekly TC genesis especially for regions west of the dateline.

The relationship between ENSO and TC activity is well known from many previous studies. Considering the relationship between ENSO and weekly TC genesis probabilities for each zone, we use the Nino3.4 index calculated from TIGGE forecasts as a predictor of weekly TC genesis. Based on the analysis, TC genesis increased east of the dateline in the warm ENSO phase years, and increased in the west in the cold ENSO phase years. This is consistent with previous studies. In the positive ENSO phase, the TC genesis is preferentially enhanced eastward to the South Pacific Ocean, with the highest TC density centered on the dateline. In the negative ENSO phase, TC genesis positions have their maximum density further west of the dateline, because equatorial convection moves further westward.

In this study, it is critical to pre-define the region of interest for the TC forecast statistical model. The selection of these regions was based on geographical and physical considerations. The boundary at 150°E provides a natural geographical separation, with relatively few TCs crossing this longitude (Kim et al. 2015). The boundary of 180°E approximately separates regions that are known to respond to ENSO, a critical driver of TC activity, in opposite ways. Forecasts using smaller zones, which would potentially be more useful, were tested with different longitude coverage for each zone. However, the models only prove skillful where there are a sufficiently dense number of TC formations. Thus, there is a trade-off between forecast skill and usefulness. In the case of employing smaller zones, the statistical model itself is not established due to all zero predictions (TC genesis) on some days. However, it is possible to further adapt this methodology to alternative zones in the future to pre-define the target regions.

The final goal of this project is to establish a TC forecast model in the Pacific Islands where TIGGE forecast data are directly collected. However, the TIGGE forecast only covers the latest 10 years from 2006, and only 92 TCs occurred during this period. This could be limiting the statistical model, because long training periods are necessary for more reliable models. In the future, it is possible to investigate an alternative way to overcome this limitation.

5 Concluding Remarks & Suggestions

5.1 Seasonal Forecast during the Austral Winter

— Through this project, we have analyzed the characteristics and skill of probabilistic forecasts of the islands in Kingdom of Tonga dry season rainfall from the APCC dynamical coupled model forecasting system, and have examined the feasibility of forecast skill improvement through statistical-dynamical prediction methods. A 99-member ensemble of hindcasts for 1983-2009 generated from the current operational version of APCC multi-model was employed for this study.

The direct probabilistic forecasts from APCC MME dynamic models for rainfall exhibit poor to moderate reliability. To examine if additional skill improvement is obtainable through statistical post-processing, we developed a statistical calibration model and a statistical bridging model that use APCC's predictions of Tonga rainfall and mean sea level pressure (MSLP) in the SH as predictors of Tonga rainfall, respectively.

The direct precipitation from the APCC model has difficulty in predicting the amount of observed precipitation, however, the forecast skill of statistical calibration is not as good overall when compared to the direct rainfall prediction from APCC over most of areas. The poorer performance of the statistical calibration model suggests that major source of errors in APCC rainfall forecasts is unlikely to be the model's systematic linear bias, which should be, in principle, be corrected statistically. This result suggests that the APCC model hindcast record is probably too short in order to develop stable statistical corrections. For instance, during the period 1983-2009 we sample only a handful of El Nino and La Nina events, which are the primary drivers of climate variability in the islands of the Pacific Ocean.

Forecast skill, as measured by ROC and BSS, from the BRDG model is lower than or similar to that from the direct rainfall prediction from APCC in most regions (Figure 17). As mentioned in the result of CALB, the poorer performance of the statistical bridging model suggests that major source of errors in APCC rainfall forecasts is unlikely to be the model's systematic linear bias. This result suggests that our hindcast record, again, is probably too short in order to develop stable statistical corrections. Also, in the case of constructing a statistical bridging model, it is difficult to find a dominant predictor variable to explain the variability of rainfall over the islands of Tonga and in all seasons. However, we believe that tropical SST might have a reasonable strong empirical relationship between Tonga rainfall and ENSO, which can potentially be considered in a future study.

During this project, we also combined the direct rainfall predictions from APCC together with both the statistically calibrated and bridged predictions to make a multi-model ensemble prediction. Our study suggests that even if statistical or statistical-dynamical forecasts are not very skillful, they can still contribute to improving seasonal forecast skill as components of a multi-model ensemble system. We believe that more complex methods of combining models (e.g., Bayesian approach) might be able to stretch the skill of the ENS further, which is worth investigating in a potential future study.

5.2 Tropical Cyclone Subseasonal and Seasonal Prediction

— During this project, we aimed to predict the seasonal TC track density over the South Pacific by combining the APCC MME dynamical prediction system with a statistical model. The hybrid dynamical-statistical model was developed for each cluster, which indicates the representative group of TC best tracks in the South Pacific. The hybrid model in each cluster uses the statistical relationship between the TCs during the austral tropical cyclone season (November–April) and the simultaneous large-scale key predictors forecasted by the APCC MME forecasts. The hybrid model also considers the lag relationship between the TCs and large-scale fields prior to the TC season especially for the regions where there is no clear simultaneous relationship.

The cross validation result from the MME hybrid model demonstrated reasonable prediction skills, with a correlation of 0.4 to 0.6 across all TC clusters in predicting the TC number between the hindcasts and observations for 1982/1983 to 2008/2009. The prediction skill of TC track density is also high in regions where there is a climatological high TC track density around the area 160°E-180°E and 20°S. The hybrid model also shows a reasonable ability in forecasting year-to-year variability of seasonal TC track density, in response to interannual SST variability in the South Pacific Ocean.

We also tried to develop a TIGGE forecast based dynamical-statistical model for predicting weekly TC genesis probability during the South Pacific Ocean active TC seasons (November-April). A distinguishing feature of this approach is that predictors are physically relevant contemporaneous seasonal large-scale environment variables derived from a dynamical TIGGE prediction. This key point is different from a pure statistical method that depends on the lag relationship with past observation records. This study identifies potential predictors associated with weekly TC genesis probability from physical consideration. In addition, the dynamical model (here, TIGGE) provides a measure of predictor accuracy.

In this study, it was critical to pre-define the region of interest for the TC forecast statistical model. The selection of these regions was based on geographical and physical considerations. The boundary at 150°E provides a natural geographical separation, with relatively few TCs crossing this longitude (Kim et al. 2015). The boundary of 180°E approximately separates regions that are known to oppositely respond to ENSO, a critical driver of TC activity. Forecasts using smaller zones, which would potentially be more useful, were tested with different longitude coverage for each zone. However, the models only prove skillful where there are a sufficiently dense number of TC formations. Thus, there is a trade-off between forecast skill and usefulness. In case of employing smaller zones, the statistical model itself is not established due to all zero predictions (TC genesis) on some days. However, it may be possible to further adapt this methodology to alternative zones in the future to pre-define the target regions.

The final goal of this project was to establish a TC forecast model in the Pacific Islands where TIGGE forecast data are directly collected. However, the TIGGE forecast only covers the latest 10 years from 2006, and only 92 TCs occurred during this period. This could be limiting the statistical model, because long training periods are necessary. In the future, we can potentially investigate an alternative way to overcome this limitation.

5.3 Tonga Climate Project Overall Conclusions

— Through our research, we have identified the following for the seasonal forecast during the Austral Winter:

1. The APCC model has difficulty in predicting direct rainfall, but has higher performance than the statistical calibration model and the BRDG model.
2. The APCC model hindcast record, 1982 to 2009, is too short in order to develop stable and statistical corrections necessary for higher skill.
3. Tropical SST may have a reasonable strong empirical relationship between Tonga rainfall and ENSO.
4. Even if statistical or statistical-dynamical forecasts are not very skillful, they can still contribute to improving seasonal forecast skill as components of a multi-model ensemble system.

For future improved seasonal forecasts during the Austral Winter, APCC would like to suggest the following topics for further research and development:

1. A study on the usage of tropical SST as a potential dominant predictor variable to explain the variability of rainfall over the islands of Tonga and in all seasons due to its strong empirical relationship between Tonga rainfall and ENSO.
2. A study on more complex methods of combining the statistical, statistical-dynamical, and APCC multi-model-ensemble models (e.g., Bayesian approach), to further stretch the skill of the ENS.

Through our research, we have identified and developed the following for the Tropical Cyclone Subseasonal and Seasonal Prediction:

1. A hybrid dynamical-statistical model (combining the APCC MME dynamical prediction system with a statistical model) for each TC cluster, using the statistical relationship between the TCs during the austral tropical cyclone season and the large-scale key predictors forecasted by the APCC MME forecasts. This model demonstrated reasonable prediction skills.
2. Developed a TIGGE forecast based dynamical-statistical model for predicting weekly TC genesis probability during the South Pacific Ocean active TC seasons (November-April).
3. Defined regions of interest for the TC forecast statistical model based o geographical and physical considerations.

For future improved Tropical Cyclone Subseasonal and Seasonal Predictions, APCC would like to suggest the following topics for further research and development:

In order to establish a system for predicting the tropical cycle (TC) activity in the South Pacific zones during week-long periods, there are three key requirements to accomplish this objective: (1) an investigation of physically meaningful and predictable weekly TC variability, (2) potential predictors associated with weekly TC variability identified based on physical considerations, and (3) develop a forecast model based on selected predictors and evaluate the model performance in predicting sub-seasonal TC activity. This can be designed as a three-year project: Year 1 - identification of potential predictors for sub-seasonal tropical cyclone genesis; Year 2 - development and verification of a model for predicting sub-seasonal tropical cyclone genesis; and Year 3 - improve the prediction model and disseminate the results, including outreach.

In this project, we focused on the identification of possible sources (i.e., potential predictors) associated with weekly TC variability based on physical considerations, which means that we have already completed year 1 of the potential three-year project. Therefore, APCC would like to recommend the following to improve Tonga's Tropical Cyclone Subseasonal and Seasonal Predictions based on the results of this project:

1. Development and verification of a model for prediction sub-seasonal tropical cyclone genesis.
2. Improve the prediction model and disseminate the results, including outreach.

References

6 References

Abawi, Y., Lianso, P., Harrison, M. and Mason, S. J. 2005: Water, Health and Early Warnings. Seasonal Climate: Forecasting and Managing Risk. A. Troccoli, M. Harrison, D. L. T. Anderson and S. J. Mason, Springer, 351-395.

Barry, R. G., and R. J. Chorley, 2003: Atmosphere, Weather and Climate. 8th ed. Routledge, 421 pp

Bougeault, P., et al., 2010: The THORPEX interactive grand global ensemble, Bull. Am. Meteorol. Soc., 91, 1059-1072. doi:10.1175/2010BAMS2853.1

Camargo, S. J., A. W. Robertson, S. J. Gaffney, P. Smyth, and M. Ghil, 2007a: Cluster analysis of typhoon tracks. Part I: General properties. J. Climate, 20, 3635–3653.

Camargo, S. J., A. W. Robertson, S. J. Gaffney, P. Smyth, and M. Ghil, 2007b: Cluster analysis of typhoon tracks. Part II: Large-scale circulation and ENSO. J. Climate, 20, 3654–3676.

Camargo S. J., A. W. Robertson, A. G. Barnston and M. Ghil, 2008. Clustering of eastern North Pacific tropical cyclone tracks: ENSO and MJO effects. Geochemistry, Geophysics and Geosystems, 9, Q06V05, doi: 10.1029/2007GC001861.

Chand, S. S., and K. J. E. Walsh, 2009: Tropical cyclone activity in the Fiji region: Spatial patterns and relationship to large-scale circulation. J. Climate, 22, 3877-3893.

Cottrill, A., A. Charles, K. Shelton, D. Jones, Y. Kuleshov, 2013: Seasonal forecast verification in the Pacific using a coupled model POAMA and the statistical model SCOPIC. CAWCR Technical Report No. 067.

Doblas-Reyes, F. J., M. Deque, and J.-P. Piedelievre, 2000: Multi-model spread and probabilistic seasonal forecasts in PROVOST. Quart. J. Roy. Meteor. Soc., 126, 2069-2088.

Dowdy, A. J., L. Qi, D. Jones, H. Ramsay, R. Fawcett, and Y. Kuleshov, 2012: Tropical cyclone climatology of the South Pacific Ocean and its relationship to El Niño-Southern Oscillation. J. Climate, 25, 6108-6122.

Frank, W. M., 1987: Tropical cyclone formation. A Global View of Tropical Cyclones, Elsberry, R. L., Ed., Office of Naval Research, pp. 53-90.

Froude, L. S. R., 2010: TIGGE: Comparison of the Prediction of Northern Hemisphere extratropical cyclones by different ensemble prediction systems, Wea. Forecasting, 25, 819-836.

Froude, L. S. R, 2011: TIGGE: Comparison of the Prediction of Southern Hemisphere extratropical cyclones by different ensemble prediction systems, Wea. Forecasting, 26, 388-398.

Gaffney, S. J., A. W. Robertson, P. Smyth, S. J. Camargo, and M. Ghil, 2007: Probabilistic clustering of extratropical cyclones using regression mixture models. Clim. Dyn., 29, 423-440.

Gottschalck, J., et al. 2010: A framework for assessing operational Madden–Julian Oscillation forecasts: A CLIVAR MJO working group project, Bull. Am. Meteorol. Soc., 91, 1247– 1258, doi:10.1175/2010BAMS2816.1.

Gray, W. M., 1979: Hurricanes: their formation, structure and likely role in the tropical circulation. In: Shaw DB (ed) Meteorology over the tropical oceans. Roy. Meteor. Soc., London, pp. 155-218.

Hagedorn, R., F. J. Doblas-Reyes, and T. N. Palmer, 2005: The rationale behind the success of multi-model ensembles in seasonal forecasting – I. Basic concept. Tellus, 57A, 219-233.

Hall, J. D., A. J. Matthews, and D. J. Karoly, 2001: The modulation of tropical cyclone activity in the Australian region by the Madden-Julian oscillation. Mon. Wea. Rev., 129, 2970-2982.

Jiang, X., D. E. Waliser, M. C. Wheeler, C. Jones, M.-I. Lee, and S. D. Schubert, 2008: Assessing the skill of an all-season statistical forecast model for the Madden-Julian oscillation. Mon. Wea. Rev., 136, 1940-1956.

Jones, D., L. M. V. Carvalho, R. W. Higgins, D. E. Waliser, and J.-K. E. Schemm, 2004: A statistical forecast model of tropical intraseasonal convective anomalies. J. Clim., 17, 2078-2095.

Kanamitsu, M., R. E. Kistler, R. W. Reynods, S.-K. Yang,J. J. Hnilo, M. Fiorino, and G. L. Potter, 2002: NCEP/DOE AMIP-II Reanalysis (R-2). Bull. Amer. Meteor. Soc., 83, 1641-1643.

Kanamitsu, M., W. Ebisuzaki, J. Woolen, S. K. Yang, J. J. Hnilo, M. Fiorni, and G. L. Potter, 2002: NCEP-DOE AMIP- II Reanalysis (R-2). Bull. Amer. Meteor. Soc., 83, 1631-1643.

Kidwell, A., T. Lee, Y.-H. Jo, X.-H. Yan: 2016: Characterization of the variability of the South Pacific Convergence Zone using satel lite and reanalysis wind products. J. Clim., 29, 1717-1732.

Kiladis, G. N., H. V. Storch, and H. V. Loon, 1989: Origin of the South Pacific Convergence Zone. J. Clim, 2, 1185-1195.

Kang, I.-S., H.-Mi. Kim, 2010: Assessment of MJO predictability for boreal winter with various statistical and dynamical models. J. Clim., 23, 2368-2378.

Kim, H.-M. and P. J. Webster, 2010: Extended-range seasonal hurricane forecasts for the North Atlantic with a hybrid dynami cal-statistical model. Geophys. Res. Lett., 37, L21705, doi:10.1029/2010GL044792.

Kim, H.-S., C.-H. Ho, J.-H. Kim, and P.-S. Chu, 2012: Track-pattern-based model for seasonal prediction of tropical cyclone activity in the Western North Pacific. J. Climate, 25, 4660-4678.

Kim, O.-Y., 2015: Cyclone-track based seasonal prediction for South Pacific tropical cyclone activity using APCC multi-model ensemble prediction. APCC 2015 Technical Report, APEC Climate Center.

Knapp, K.R., M.C. Kruk, D.H. Levinson, H.J. Diamond, and C.J. Neumann, 2010: The International Best Track Archive for Climate Stewardship (IBTrACS). Bull. Amer. Meteor. Soc., 91, 363-376; doi: 10.1175/2009BAMS2755.1.

Kossin, J. P., S. J. Camargo, and M. Sitkowski, 2010: Climate modulation of North Atlantic hurricane tracks. J. Climate, 23, 3057-3076.

Kuleshov, Y., L. Qi, R. Fawcett, and D. Jones, 2009: Improving preparedness to natural hazards: Tropical cyclone prediction for the Southern Hemisphere, in Advances in Geosciences, 12 Ocean Science, (Ed. Gan, J.), World Scientific Publishing, Sin gapore, 127-143.

Leroy, A., and M. C. Wheeler, 2008: Statistical prediction of weekly tropical cyclone activity in the southern Hemisphere. Mon. Wea. Rev., 136, 1083-1103.

Lim, E. P., H. H. Hendon, D. L. T. Anderson, A. Charles, O. Alves, 2011: Dynamical, statistical-dynamical, and multimodel ensemble forecasts of Australian spring season rainfall. Mon. Wea. Rev., 139, 958-975.

Lin, H., G. Brunet, J. Derome, 2008: Forecast skill of the Madden-Julian Oscillation in Two Canadian Atmospheric Models, Mon. Wea. Rev., 136, 4130– 4149, doi:10.1175/2008MWR2459.1.

Lintner, B. R., J. D. Neelin, 2008: Eastern margin variability of the South Pacific Convergence Zone. Geophys. Res. Lett. 35, L16701.

Lo, F., and H. H. Hendon, 2000: Empirical extended-range prediction of the Madden-Julian oscillation. Mon. Wea. Rev., 128, 2528-2543.

Madden, R. A., and P. R. Julian, 1994: Observations of the 40-50-day tropical oscillation – A review. Mon. Wea. Rev., 122, 814-837.

Maloney, E. D., and D. L. Hartmann, 2000: Modulation of eastern North Pacific hurricanes by the Madden-Julian oscillation. J. Climate, 13, 1451-1460.

Matsueda, M., H. Endo, 2011: Verification of medium-range MJO forecasts with TIGGE. Geo. Res. Lett., 38, L11801, doi:10.1029/2011GL047480.

Mo, K. C., Paegle J. N, 2001: The Pacific-South American Modes and their downstream effects. Int. J Climatology, 21, 1211-1229.

Mo, K. C., Higgins R. W., 1998: The Pacific-South American Modes and Tropical Convection during the Southern Hemisphere Winter, 126, 1581-1596.

Palmer, T., A. Alessandri, U. Andersen, P. Cantelaube, M. Davey, P. Delecluse, M. Deque, E. Diez, F. J. Doblas-Reyes, H. F. nd R. Graham, S. Gualdi, J.-F. Gueremy, R. Hagedorn, M. Hoshen, N. Keenlyside, M. Latif, A. Lazar, E. Maisonnave, V. Marletto, A. P. Morse, B. Orfila, P. Rogel, J.-M. Terres, and M. C. Thomson, 2004: Development of a European multimodel ensemble system for seasonal-to-interannual prediction (DEMETER). Bull. Amer. Meteor. Soc., 85, 853–872.

Ramsay, H. A., L. M. Leslie, P. J. Lamb, M. B. Richman, and M. Leplastrier, 2008: Interannual variability of tropical cyclones in the Australian region: Role of large-scale environment. J. Climate, 21, 1083-1103.

Ramsay, H. A., S. J. Camargo, and D. Kim, 2012: Cluster analysis of tropical cyclone tracks in the Southern Hemisphere. Clim. Dyn., 39, 897-917.

Salinger, M. J., R. E. Basher, B. B. Fitzharris, J. E. Hay, P. D. Jones, J. P. Macveigh, I. Schmidely-Leleu, 1995: Climate trends in the South-west Pacific. Int. J. Climatology, 15, 285-302.

Seo, K. H., W. Wang, J. Gottschalck, Q. Zhang, J.-K. E. Schemm, W. R. Higgins, and A. Kumar, 2009: Evaluation of MJO forecast skill from several statistical and dynamical forecast models. J, Clim, 22, 2372-2388.

Su, X. H. Yuan, Y. Zhu, Y. Luo, and Y. Wang, 2014: Evaluation of TIGGE ensemble predictions of Northern Hemisphere summer precipitation during 2008-2012. J. Geophys. Res. Atmos., 199, 7292-7310.

Thompson, D. W. J. and J. M. Wallace, 2000: Annular modes in the extratropical circulation. Part I: Month-month variability. J. Climate, 13, 1000-1016.

Vincent E. M., M. Lengaigne, C. E. Menkes, N. C. Jourdain, P. Marchesiello, G. Madec, 2009: Interannual variability of the South Pacific Convergence Zone and implications for tropical cyclone genesis. Clim. Dyn., 36, 1881-1896.

Waliser, D. E., C. Jones, J. K. E. Schemm, and N. E. Graham, 1999: A statistical extended-range tropical forecast model based on the slow evolution of the Madden-Julian oscillation. J. Climate, 12, 1918-1939.

Wang, H., J. K. E. Scheme, A. Kumar, W. Wang, L. Long, M. Chelliah, G. D. Bell, and P. Peng, 2009: A statistical forecast model for Atlantic seasonal hurricane activity based on the NCEP dynamical seasonal forecast, J. Climate, 22, 4481-4500.

Werner, A., and N. J. Holbrook, 2011: A Bayesian forecast model of Australian region tropical cyclone formation. J. Climate, 24, 6114-6131.

Wilks, D., 2006: Statistical Methods in the Atmospheric Sciences. Academic Press, 592 pp.

WMO, 2014: Tropical cyclone operational plan for the South Pacific and South-East Indian Ocean. World Meteorological Organi zation Technical Document, Report No. TCP-24.

WMO, 2005: THORPEX, WMO-No. 978, 15 pp., Geneva, Switzerland.

Zebiak, S. E., 2003: Research potential for improvements in climate prediction. Bull. Amer. Meteor. Soc., 84, 1692-1696.

Zhang, L, H. Ma, L. Wu, 2016: Dynamics and mechanisms of decadal variability of the Pacific-South America mode over the 20th century. Clim. Dyn. 46, 3657-3667.

APEC Climate Center 12 Centum 7-ro Haeundaegu Busan 612-020 Tel: +82-51-745-3900 Fax: +82-51-745-3949 www.apcc21.org

www.facebook.com/apcc21 www.twitter.com/apcc21 www.flickr.com/apcc21 www.youtube.com/APECClimateCenter www.plus.google.com/+APECClimateCenter21